SANDIA REPORT
SAND2004-4320
Unlimited Release
Printed September 2004

RESPONSE OF REMOVABLE EPOXY FOAM EXPOSED TO FIRE USING AN ELEMENT DEATH MODEL

Michael L. Hobbs

Prepared by
Sandia National Laboratories
Albuquerque, New Mexico 87185 and Livermore, California 94550

Sandia is a multiprogram laboratory operated by Sandia Corporation,
a Lockheed Martin Company, for the United States Department of Energy's
National Nuclear Security Administration under Contract DE-AC04-94AL85000.

Issued by Sandia National Laboratories, operated for the United States Department of Energy by Sandia Corporation.

Available to DOE and DOE contractors from
U.S. Department of Energy
Office of Scientific and Technical Information
P.O. Box 62
Oak Ridge, TN 37831

Telephone: (865) 576-8401
Facsimile: (865) 576-5728
E-Mail: reports@adonis.osti.gov
Online ordering: http://www.doe.gov/bridge

Available to the public from
U.S. Department of Commerce
National Technical Information Service
5285 Port Royal Rd
Springfield, VA 22161

Telephone: (800) 553-6847
Facsimile: (703) 605-6900
E-Mail: orders@ntis.fedworld.gov
Online order: http://www.ntis.gov/help/ordermethods.asp?loc=7-4-0#online

SAND2004-4320
Unlimited Release
Printed September 2004

RESPONSE OF REMOVABLE EPOXY FOAM EXPOSED TO FIRE USING AN ELEMENT DEATH MODEL

Michael L. Hobbs
Engineering Sciences Center
Sandia National Laboratories
P.O. Box 5800
Albuquerque, New Mexico 87185-0836

Abstract

Response of removable epoxy foam (REF) to high heat fluxes is described using a decomposition chemistry model [1] in conjunction with a finite element heat conduction code [2] that supports chemical kinetics and dynamic radiation enclosures. The chemistry model [1] describes the temporal transformation of virgin foam into carbonaceous residue by considering breakdown of the foam polymer structure, desorption of gases not associated with the foam polymer, mass transport of decomposition products from the reaction site to the bulk gas, and phase equilibrium. The finite element foam response model considers the spatial behavior of the foam by using measured and predicted thermophysical properties in combination with the decomposition chemistry model. Foam elements are removed from the computational domain when the condensed mass fractions of the foam elements are close to zero. Element removal, referred to as element death, creates a space within the metal confinement causing radiation to be the dominant mode of heat transfer between the surface of the remaining foam elements and the interior walls of the confining metal skin. Predictions were compared to front locations extrapolated from radiographs of foam cylinders enclosed in metal containers that were heated with quartz lamps [3,4]. The effects of the maximum temperature of the metal container, density of the foam, the foam orientation, venting of the decomposition products, pressurization of the metal container, and the presence or absence of embedded components are discussed.

Intentionally left blank

Acknowledgements

I would like to acknowledge the technical and management assistance provided by numerous colleagues at Sandia National Laboratories and Brigham Young University. Many colleagues have contributed data and technical advice regarding foam response modeling; I am grateful to them all and apologize if I have inadvertently failed to acknowledge them in print. Gene Hertel, Martin Pilch, Mike Prairie, and Art Ratzel provided management support and funding. Steve Bova helped debug the multi-processor dynamic pressurization implementation in CALORE. Robert Kerr helped make the finite element meshes. Dan Clayton, Ken Erickson, and Tom Fletcher provided data from various small-scale experiments. Ted Borek, Jaime Castañeda, Paige Jackson, Jill Miller, and Anita Renlund also contributed to the laboratory-scale experimental program. Terry Aselage, Ken Erickson, Walt Gill, and Amy Sun provided thermophysical properties. John Bentz, T. Y. Chu, and Jack Pantuso developed the basic experimental technique for the radiant heat experiments and completed the first two series of experiments. Dean Dobranich, Kevin Dowding, Ken Erickson, Brian Rutherford, Amy Sun, and Steve Trujillo helped in providing the final radiant heat experimental designs. Ken Erickson and Steve Trujillo coordinated the final radiant heat experiments along with Ben Belone, Chuck Hanks, David Ho, Mike Ramirez, and Tomás Sánchez who ran the final radiant heat tests. Jim Nakos coordinated activities at the Radiant Heat Facility. John Oelfke instrumented the samples for the final radiant heat experiments. Jo Bridge and Paul Thompson helped fabricate the final radiant heat experiments. Ed Russick and Jim Aubert provided the REF samples. Mike Hassard, Jerry Stoker, Kyle Thompson, and Steve Younghouse obtained the x-ray images. Kyle Thompson and Jeremy Barney organized the x-rays for comparison to model predictions. Student interns, David Darrow, Kevin Grossarth, and Scot Waye helped extract the decomposition fronts from the x-ray images and overlay them onto various simulations. I am also thankful for technical advice provided by Gene Hertel, Roy Hogan, and Marvin Larsen during the preparation of this manuscript.

Intentionally left blank

Table of Contents

Table of Contents

Intentionally left blank

List of Figures and Tables

Executive Summary

A simple decomposition chemistry and foam response model (SREF) has been developed to predict the decomposition behavior of a closed-cell, rigid, thermally removable, epoxy foam (REF) used to encapsulate shock and vibration sensitive components. The decomposition chemistry model has been described in detail in a previous report [1] and is only summarized in the current report. The primary emphasis of the current report is to describe an element-death-based foam response model that may be applicable to abnormal thermal environments such as fire. "Response" refers to the velocity, position and shape of the decomposition front surface driven by the foam polymer breaking into small fragments that vaporize. Response also refers to the ability of the degrading foam to thermally protect encapsulated components as well as pressurize sealed systems.

Initially, embedded components do not increase in temperature appreciably even though the temperature of the confining metal skin may be at flame temperatures. The delayed response of embedded components to high temperature is attributed to the low thermal conductivity of the foam, which causes steep temperature gradients at the decomposition font. Eventually, the decomposition front uncovers or exposes embedded components to the hot metal skin, which exchanges energy via radiation. View factors are computed dynamically as the foam disappears creating a clean enclosure filled with nonparticipating gases. In real systems, clean enclosures may not be produced. Instead, the enclosure may be filled with foam residue that may participate with radiation heat transport. Participating media radiation is not addressed in the current report.

The foam response is modeled with a finite element code that solves the heat diffusion equation with a source term for the endothermic decomposition chemistry [2]. The chemistry model also provides the time-resolved mass fraction of the condensed-phase and gas-phase decomposition products within each element. Foam elements are removed from the computational domain when the condensed-phase mass fraction approaches zero or when the condensed-phase becomes a low-viscosity liquid that flows. Element

removal, referred to as element death, creates a space within the metal confinement causing radiation to be the dominant mode of heat transfer between the surface of the remaining foam elements and the interior walls of the confining skin. The radiation boundary conditions are inherited by the underlying elements and viewfactors are recalculated whenever elements are removed. Element death is an *ad hoc* method of tracking the decomposition front and defining the dynamic radiation enclosure. One problem with element death is that the solution depends on the grid size. Grid independence was demonstrated when characteristic element dimensions were 0.1-cm or smaller.

The foam response model was evaluated with four series of radiant heat experiments [3] run over a two year period: 1) AF series [April 2001-July 2001], 2) REF series [March 2002], 3) TUNA series [October 2002], and 4) V series [April 2003]. The AF, REF, and TUNA series were run to show the effect of sample orientation for various boundary temperatures at ambient pressure, regulated pressure, and dynamic pressure, respectively. The "V" series of unconfined, ambient pressure experiments were run at two temperatures and various orientations to assess the repeatability of the radiant heat experiments and to evaluate the validity of the foam response model. The validity and uncertainty associated with the element death response model was evaluated by others and is not discussed in this report. The first three series considered a total of 17 experiments and the V series considered 16 experiments, for a total of 33 experiments.

Decomposition of removable epoxy foam (REF) formed more liquids than decomposition of unconfined polyurethane foam at similar conditions [5-7]. The REF experiments exposed to lower temperatures developed slower and thicker fronts than REF experiments at higher temperatures. Three orientations of the incident thermal fluxes were considered: top-, bottom-, and side-heated. The top- and bottom-heated fluxes were parallel to the gravity vector, but opposite in direction. The side-heated experiments were perpendicular to the gravity vector. The bottom-heated and side-heated experiments were prone to liquid flowing from the decomposition front. The effect of liquid formation was most significant when the vol-

ume of the foam was large (AF series and REF series). Liquid effects were not as significant for the experiments where the volume of foam was small (TUNA series and V series).

Foam response is not only complicated by liquid formation and flow, but liquids may also penetrate the thermally damaged material and cause enhanced front movement due to preheating and liquefaction or dissolution of the foam polymer by decomposition generated solvents. The foam response model does not solve the momentum equation for polymer flow and does not explicitly consider liquefaction. However, flow effects were treated empirically with limited success for systems with large amounts of foam such the AF and REF series. The empiricism was used when the orientation of the decomposition front caused gravity-induced flow from the interface.

Elements were removed early to mimic flow effects in systems that produced significant liquid volumes at orientations that favored gravity-induced flow. Elements were removed when the solid mass fraction was less than 0.75 (point where the foam is assumed to be a low viscosity liquid) for bottom- and side-heated experiments to prevent liquid accumulation at the decomposition front. The decomposition fronts were thin and propagated at increased velocities similar to the observed front velocities of the AF and REF experiments. However, the empirical model did not predict the curved shape of the observed front, which appeared thinner in the middle of the foam and thicker near the sides of the confinement. The empirical flow model did not provide much improvement for systems that did not produce significant volumes of liquid at the decomposition fronts such as the TUNA and AF series. The empirical model is not recommended for use with systems that do not generate significant volumes of liquids, such as observed in the TUNA or AF experiments.

The smallest differences between measured and predicted front locations were for the ambient pressure top-heated experiments where gravity-induced flow and liquid penetration were minimal. The largest differences between measured and predicted front locations were for the top-heated experiments at elevated pressure. For these elevated pressure experiments, hot liquids may have penetrated the degrading

foam causing increased heat transfer and subsequent liquefaction of the unreacted polymeric foam. The bottom-heated and side-heated experiments gave reasonable agreement with the predictions even at elevated pressures since liquids did not accumulate at the decomposition front and penetration and secondary liquefaction were minimized.

Besides front location, the measured pressures in two of the fully confined TUNA experiments were used to evaluate the foam response model. For these simulations, the foam responses were calculated using faster rates determined from unconfined thermogravimetric analysis (TGA) experiments and slower rates obtained from confined TGA results. Not only were the front locations predicted better, but also the predicted pressures were much closer to the measured pressures using the *faster rates obtained from unconfined TGA* results, even though the TUNA experiments were fully-confined. Confinement effects are different in the component-scale experiments than in the small-scale TGA experiments. Decomposition gases are confined locally in the small-scale TGA experiments. Decomposition gases are not constrained to be in local contact with the degrading foam in the radiant heat experiments.

The V experiments were used to access the ability of the foam response model to predict the temperature in embedded components. Replicate experiments were used to access the uncertainty in the component temperatures. The largest discrepancy in the component temperatures between replicate experiments was about 50ºC. The model predictions were within the measurement uncertainty for locations in the components that were dominated by conduction. However, the model predictions were always higher than the measured temperatures when the mode of heat transfer was dominated by the foam response. The predicted temperatures were about 25°C higher than the measurement for the experiments with boundary temperatures of 750°C. The predicted temperatures were about 100°C higher than the measurement for the experiments with boundary temperatures of 900°C. This discrepancy may be attributed to significant residue left in the enclosure. Postmortem photographs showed that the decomposition-generated enclosure was

filled with layers of degraded foam residue. The residue may act as a barrier to heat transfer, which was not included in the element death model.

In summary, an element-death-based foam response model has been developed using the SREF decomposition chemistry model with decomposition rates based on TGA experiments. Thermophysical properties were based on experimental data up to about 140°C. Above 140°C, reaction enthalpy effects interfered with data interpretation and thermophysical properties were estimated. The foam heat capacity was assumed to vary linearly with temperature to 70°C. Above 70°C, the heat capacity was assumed to be constant and asymptotically approached pyrolytic graphite at higher temperatures. The thermal conductivity was assumed to be slightly dependent on density at room temperature. At 250°C, the thermal conductivity was assumed to be the same as the thermal conductivity of the REF polymer regardless of the initial density of the foam. Above 250°C, the thermal conductivity was assumed to be constant. Confinement effects were shown to be different in the larger-scale experiments than in the small-scale TGA experiments. Gases were assumed to be transparent and were permitted to either leave or remain in the system. The system pressure was either set to a predetermined level, or a pressurization model was used to predict pressure due to gas accumulation. The response model was compared to various component-scale experiments. Gravity induced flow was significant for experiments composed of large amounts of foam. The model predicted embedded component temperatures that were 5-100°C too high. The higher predicted temperatures were attributed to neglecting residue accumulation in the developing enclosure.

Intentionally left blank

RESPONSE OF REMOVABLE EPOXY FOAM EXPOSED TO FIRE USING AN ELEMENT DEATH MODEL

1. Introduction and Background

This report describes a simple removable epoxy foam (SREF) response model developed to predict the decomposition behavior of removable epoxy foam (REF) exposed to fire-like heat fluxes. REF is a closed-cell rigid epoxy foam that is composed of various moieties derived from pentaerythritol triacrylate, nonyl phenol, dimethyldicyane, bisphenol A, and a removable epoxy resin as shown in Fig. 1. The acronym SREF refers to a foam response model as well as a decomposition chemistry model that was described in detail in a previous report [1]. REF is used to encapsulate shock, vibration, and temperature sensitive components within metal enclosures, which may have cable openings that provide pathways for the decomposition gases to exit the system or may be hermetically sealed to prevent gases from entering or exiting the system. Consequently, the decomposition model must be able to predict mass loss in unconfined systems as well as closed systems that may pressurize.

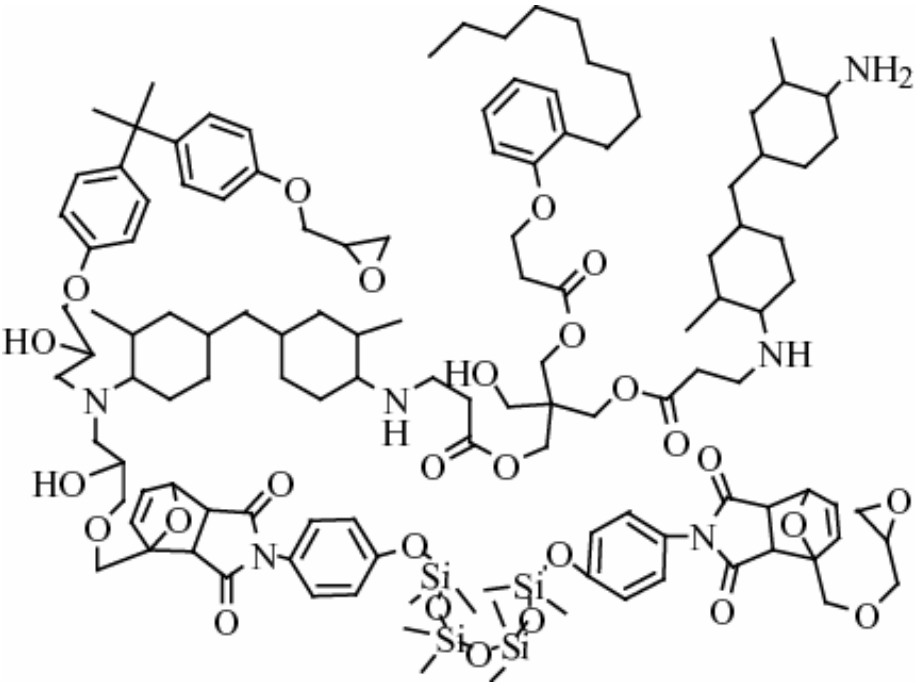

Fig. 1 Most common chemical structural unit of the REF polymer [1]

Traditional encapsulants have not been designed for easy removal. These encapsulants were difficult to remove because of their cross-linking, solvent resistance, and mechanical toughness. Such encapsulants were removed for component maintenance by using aggressive solvents and/or mechanical chiseling, which can easily damage electronic assemblies. McElhanon et al. [8] have recently patented a method to make thermally removable epoxies that can be removed from potted assemblies with a mild solvent (e.g., n-butanol) at 90ºC. Removability was achieved by incorporating chemically labile linkages within the cross-linked polymeric network using the reversible Diels-Alder reaction. The reverse (retro) Diels-Alder reaction is favored by heating the polymeric foam to temperatures near 90ºC and a mild solvent promotes dissolution of the foam.

The SREF chemistry model [1] was developed specifically for removable epoxy foam referred to as REF100 [8]. However, the formulation for the REF foam has evolved in order to increase the glass transition temperature to be well above normal design operating temperatures. Two additional formulations, referred to as REF200 and REF300, differ in the amount of blowing and curing agents used in the synthesis. Rather than develop separate models for each new series of foam, a single mechanism was developed to describe decomposition of all three removable epoxy foam types [1]. Decomposition of REF100, REF200, and REF300 type foam has been modeled using the same kinetic coefficients. The only differences in the chemistry model are the initial constituents making up the polymeric foam. In the foam response model, element death criterions used to propagate the decomposing foam surface are different for the three formulations since the ultimate residue fractions differ for each type of foam.

The SREF response model discussed in the current report is based on concepts from several polyurethane foam response models developed previously [5-7], which use “element death” to describe the regressing surface of the foam exposed to high heat fluxes. “Element death” is used to describe removal of elements from the computational domain when the solid mass fractions within elements approach zero. The dominant mode of heat transfer changes from conduction to radiation when elements are removed.

Energy is transferred by radiation from the hot surface of the metal confinement walls to the decomposing foam surface. Element death is also used as an empirical model to simulate the effects of flow for conditions favoring liquid formation.

Decomposing foams do not always leave clean enclosures containing transparent gases. Partially reacted foam residue can fill the enclosure. For example, intumescent foams, similar to pyrotechnic snakes, are designed to leave residues in the enclosure for fire protection. Postmortem analysis [3] of component-scale experiments with REF shows layered structures within the enclosure after the foam had been exposed to high heat fluxes. The mechanism and kinetics of this layer formation is not known. The structure and composition of the residue *in situ* is not known. The layered residue structures in the enclosures are not addressed in the current report.

This report briefly describes the SREF foam decomposition chemistry model [1], which is used to drive the foam response model. The report also describes the implementation of the decomposition chemistry model into a three-dimensional thermal diffusion finite element computer code that includes finite rate kinetics with enclosure radiation [2], thermophysical properties, and element death. Model predictions are compared to four separate series of radiant heat experiments [3]. The report ends with a summary and conclusion section.

Intentionally left blank

2. Decomposition Chemistry Model

The decomposition chemistry model is described in detail in [1] and is only summarized in this section. The decomposition chemistry model was developed to predict the decomposition behavior of epoxy foam composed of an epoxy polymer, blowing agent, and surfactant. The chemistry model is based on a simple four-step mass loss model using distributed Arrhenius reaction rates. A single reaction was used to describe desorption of the blowing agent and surfactant (BAS). Three reactions were used to describe degradation of the polymer. The coordination number of the polymeric lattice was determined from the chemical structure of the polymer; and a lattice statistics model was used to describe the evolution of polymer fragment populations.

The model lattice was composed of sites connected by octamethylcylotetrasiloxane (OS) bridges, mixed product (MP) bridges, and bisphenol-A (BPA) bridges. The mixed products were treated as a single species, but are likely composed of phenols, cresols, and furan-type products. Eleven species are considered in the SREF model – 1) BAS, 2) OS, 3) MP, 4) BPA, 5) 2-mers, 6) 3-mers, 7) 4-mers, 8) nonvolatile carbon residue, 9) nonvolatile OS residue, 10) L-mers, and 11) XL-mers. The first seven of these species (VLE species) can either be in the condensed-phase or gas-phase as determined by a vapor-liquid equilibrium model based on the Rachford-Rice equation [1]. The last four species always remain in the condensed-phase.

The 2-mers, 3-mers, and 4-mers are polymer fragments that contain two, three, or four sites, respectively. The residue can contain C, H, N, O, and/or Si. The L-mer fraction consists of polymer fragments that contain at least five sites (5-mer) up to a user defined maximum mer size (max-mer). The XL-mer fraction consists of polymer fragments greater than the max-mer and can contain the infinite lattice if the bridge population is less than the critical bridge population. The decomposition chemistry model predicts solid mass fraction based on the thermal history, the degree of confinement of decomposition gases, and the thermodynamic pressure of the system. Parameters for the chemistry model, including reaction

enthalpy and specific heat, are given in reference [1]. The interested reader can also find more information regarding the chemistry model in reference. [1].

The mean activation energies and distribution parameters were listed incorrectly in Table 7 of [1]. The correct values are given in Table 1 and were used for the simulations discussed in the current report as well as the simulations in [1]. The four Arrhenius prefactors (A_i), 1×10^{13}, 2×10^{15}, 2×10^{16}, and 6×10^{12} were listed correctly in [1]. The kinetic parameters listed in Table 7 of reference. [1] give similar mass loss predictions. However, the predictions of the condensed-phase and gas-composition are not as accurate. Accurate gas-phase compositions are needed for pressurization predictions.

Table 1. Kinetic Parameters

ξ_i	μ_i	σ_i	Units
A_1	1×10^{13}	NA	1/s
A_2	2×10^{15}	NA	1/s
A_3	2×10^{16}	NA	1/s
A_4	6×10^{12}	NA	1/s
E_1	28.7	0.761	Kcal/mol
E_2	46.4	1.082	Kcal/mol
E_3	58.1	0.513	Kcal/mol
E_4	43.5	1.910	Kcal/mol
σ_{E1}	0.76	0.297	Kcal/mol
σ_{E2}	2.80	0.426	Kcal/mol
σ_{E3}	6.60	0.922	Kcal/mol
σ_{E4}	0.79	1.010	Kcal/mol

Erickson et al. [3] measured the rate of mass loss from 2.5-mg REF samples heated at 20ºC/min in two different 4-mm diameter sample pans. One of the sample pans was uncovered (unconfined) and the other sample pan had a lid with a 0.06-mm orifice (confined). The rate of mass loss from these two ex-

periments was significantly different with the mass loss rate of the "unconfined" experiment being greater than the mass loss rate of the "confined" experiment. Differences in these two rates were empirically modeled with the SREF chemistry model [1] by using a mass transport coefficient that was proportional to the orifice diameter. Rather than trying to relate the TGA orifice diameter to the larger-scale radiant heat experiments, the rates determined from the "unconfined" and "confined" TGA experiments were used as bounds on the decomposition rates. Rates derived from the unconfined TGA data are referred to in the current work as the "faster" rates. Rates derived from the confined TGA rates are referred to as the "slower" rate model. Erickson et al. [3] gives more detail on the laboratory-scale TGA experiments and the effects of confinement.

All of the radiant heat experiments were simulated with both the slower and faster rate models. None of the predictions using the slower rates matched the front locations implied by the radiographs and are not presented in the current report. Furthermore, predictions based on the "slower" rates obtained from confined TGA experiments [3] did not match pressurization rates in the TUNA experiments and the embedded component temperature in the V experiments. These preliminary simulations suggest that the confinement effects observed in the smaller TGA experiments *do not scale*. Predictions that used the faster rates associated with the unconfined TGA experiments [3] were always closer to the experimental observations than simulations performed using the slower rates associated with the confined TGA experiments. The TGA experiments considered local confinement where the decomposition products were kept in local contact with the degrading foam. In the larger experiments, decomposition products were not locally constrained.

Intentionally left blank

3. Element Death Response Model

The response of the foam encapsulant was determined with a finite element model (FEM) that solves the heat diffusion equation with a source term for chemistry [2].

$$\rho C \frac{\partial T}{\partial t} = \frac{\partial}{\partial x}\left(k \frac{\partial T}{\partial x} \right) + \sum_{i=1}^{4} q_i r_i \,, \tag{1}$$

where ρ, C, T, t, x, k, q, and r represent material density, specific heat, temperature, time, spatial coordinate, thermal conductivity, endothermic energy release, and reaction rate, respectively. The subscript "i" in eqn (1) represents the four SREF reactions. The reaction rates and reaction enthalpies are discussed more in [1]. Enclosure or surface-to-surface radiation was calculated by solving the following radiation enclosure equation:

$$\sum_{j=1}^{N}\left[\frac{\delta_{kj}}{\varepsilon_j} - F_{k-j}\left(\frac{1-\varepsilon_j}{\varepsilon_j} \right) \right] \frac{Q_j}{A} = \sum_{j=1}^{N}\left(\delta_{kj} - F_{k-j} \right) \sigma T_j^4 \,. \tag{2}$$

Q represents the energy transfer between surfaces in an enclosure where δ_{kj} is the unit tensor, σ is the Stefan-Boltzmann constant, ε is the emissivity, and F_{k-j} are radiation view factors defined as the fraction of energy leaving surfaces j and arriving at surface k. Q is treated as a boundary condition in eqn (1).

Solution of the FEM equations gives the time-resolved temperature within the foam and inert materials such as the confining metal skin and the embedded components. Species continuity equations are solved to obtain species concentrations and solid fraction as discussed further in [1]. The boundary temperatures of the high-conductivity skin were specified. The response model generates clean enclosures as discrete foam elements are removed from the computational domain when the calculated solid mass fraction within these elements approached zero or when the condensed-phase becomes a low-viscosity liquid that flows. Upon element removal, radiation boundary conditions were reapplied to exposed elements and viewfactors were recomputed. A major assumption is that the developing enclosure is filled with nonparticipating gases. Another tenuous assumption is that element death implicitly allows removal of nonvolatile residues, which can be as much as 20% by mass of the initial foam.

Thermophysical properties are needed to determine foam response. The initial foam densities were determined from the initial sample volume and mass. Initial temperatures were measured using embedded thermocouples for some of the experiments and were nominally at 25ºC. The foam emissivity was taken to be 0.8 since materials with rough surfaces typically have emissivities that approach unity. Reaction enthalpy was measured with a differential scanning calorimeter and was discussed in detail in reference [1]. Specific heat and thermal conductivity were measured at several laboratories [9-11].

3.1 Specific Heat

Figure 2 shows measured specific heat of the removable epoxy foam [9-11], specific heat of pyrolytic graphite [12], and the specific heat used in the SREF model [1]. The circles represent Dobranich and Gill's data [9] up to about 100ºC. Aselage [10] performed four experiments all with the same sample. In Fig. 2., Aselage's initial run is represented in the legend with a "1." Subsequent experiments are represented with "2", "3", and "4." One problem with running the same sample with a decomposing material is that almost half of the initial sample mass decomposes at 350ºC as discussed in [1]. Furthermore, the specific heat data in Fig. 2 were evaluated without considering reaction enthalpies. Neglecting reaction enthalpy is acceptable provided the sample temperatures remain below significant reaction thresholds. Only specific heat data up to the glass transition temperature is considered in the current report to avoid confounding sensible enthalpy with reaction enthalpy effects.

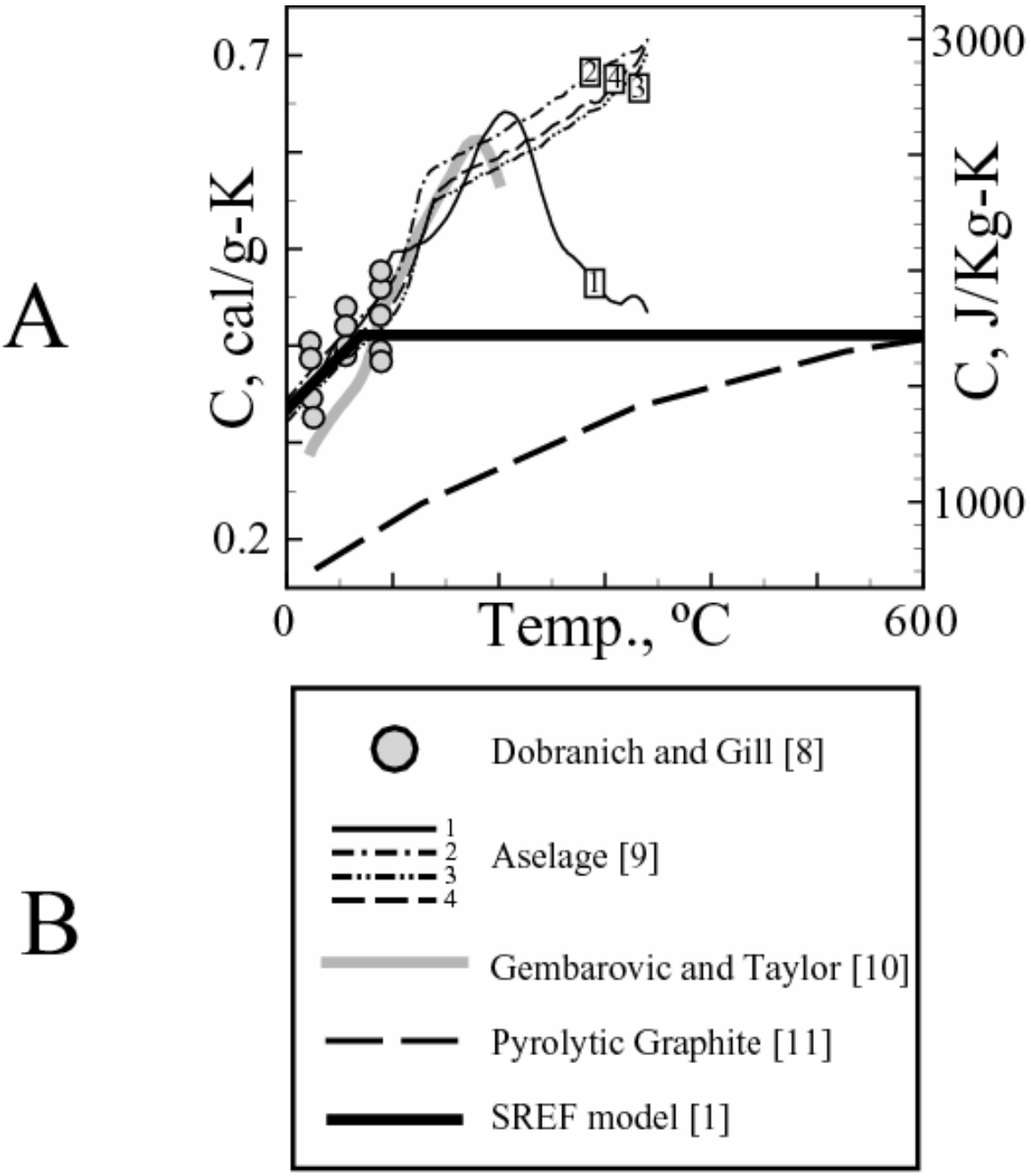

Fig. 2 A) Measured heat capacity for removable epoxy foam and pyrolytic graphite. The thick black solid line is the heat capacity used in the SREF chemistry model to obtain reaction enthalpy. B) Legend for the plot in A.

The SREF specific heat model, shown in Fig. 2 as a thick black line, is

$$C = \begin{cases} 0.0011T + 0.033535 & T < 343.15\,\text{K} \ \ (70°\text{C}) \\ 0.411\dfrac{cal}{g\text{-}K} & T \geq 343.15\,\text{K} \ \ (70°\text{C}) \end{cases} \tag{3}$$

where C and T represent specific heat in cal/g-K and temperature in K, respectively. The specific heat is assumed to follow Aselage's data up to the glass transition temperature, which is about 70ºC for REF100 [8]. The glass transition temperature is higher for REF200 and REF300; however, the specific heat is assumed to be the same for these two types of foams. The specific heat is assumed to be constant for temperatures greater than 70ºC. The pyrolytic graphite specific heat converges to the constant SREF specific heat value at high temperatures where the degraded foam consists primarily of nonvolatile residues with high carbon content.

3.2 Thermal Conductivity

Figure 3.A shows the measured thermal conductivity as a function of density and temperature [9,11]. Measured thermal conductivities did not vary significantly with temperature. The thermal conductivity used with the element death foam response model is plotted in Fig. 3.B and labeled as "SREF." The model thermal conductivity at 25ºC depends slightly on density as follows:

$$k_{25°\text{C}} = 1.65\times10^{-4}\,\rho_f + 5.67\times10^{-5}\ \text{cal/s-cm-K}, \tag{4}$$

where ρ_f is the bulk foam density in g/cm^3. At 250ºC, the SREF response model thermal conductivity is assumed to be equal to the average thermal conductivity of the pure polymer:

$$k_{250°\text{C}} = 4.36\times10^{-4}\ \text{cal/s-cm-K}. \tag{5}$$

The thermal conductivity is assumed to vary linearly with temperature between the thermal conductivity at 25ºC and the thermal conductivity at 250ºC. When the foam temperature exceeds 250ºC, the thermal conductivity is assumed to be independent of temperature at a value of 4.36×10^{-4} cal/s-cm-K (0.183 W/m-K).

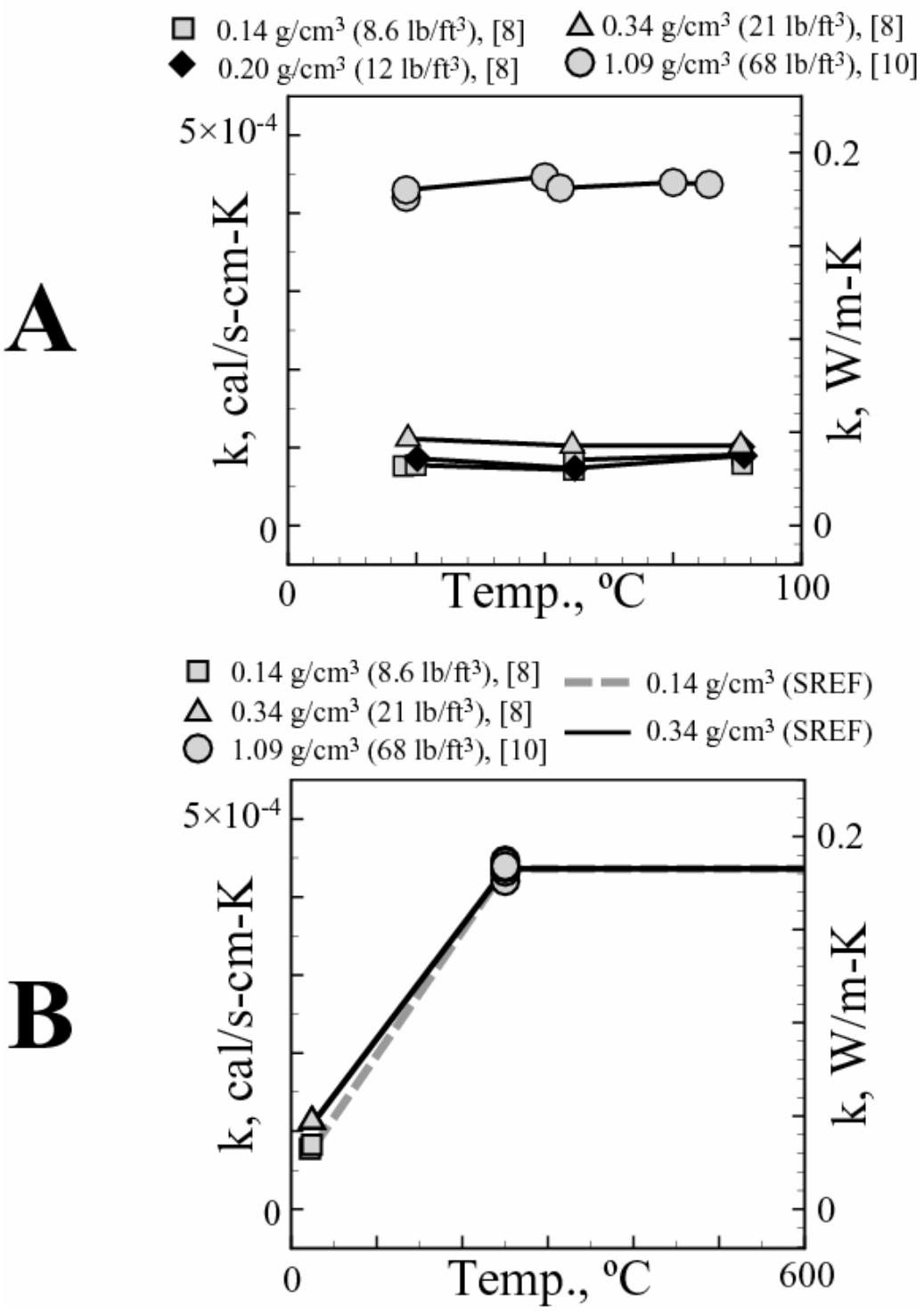

Fig. 3. A) Measured thermal conductivity of removable epoxy foam between 20 and 90ºC. B) Measured thermal conductivity (symbols) and thermal conductivity used in the SREF "element death" based response model (lines).

The form of the thermal conductivity used with the element death response model is based loosely on several experimental observations. In the AF radiant heat experiments, real time x-ray images were used with temperature measurements to make several general observations: 1) the thermocouples started to move near the glass transition point for REF100 (70ºC) indicating softening of the polymer and 2) the slope of the temperature gradient changed near 250ºC consistent with liquefaction observed in the small-scale experiments [3]. The foam thermal conductivity for foam temperatures greater than or equal to 250ºC was assumed to be the same as the thermal conductivity of the polymeric plastic (1.09 g/cc) without gas bubbles as measured by Gembarovic and Taylor [11].

The thermal conductivities of most liquids decrease with increasing temperature, except for aqueous solutions, water, and some multihydroxy and multiamine molecules [13]. Bubble formation may also contribute to an increased thermal conductivity due to convective transport. It is not clear whether thermal conductivity should increase or decrease when the polymer temperature exceeds 250ºC since the polymer degradation products contain multihydroxy and multiamine molecules. Since opposing factors may lead to increasing or decreasing thermal conductivity, the liquid thermal conductivity for the element death response model was assumed to be independent of temperature. The assumed form of the thermal conductivity model is likely inaccurate since radiative transport starts to dominate as the condensed-phase transforms into a gas. More work is needed to estimate thermophysical properties of degrading materials, which is beyond the scope of the current report.

3.3 Density

To properly account for changes in density with reaction, a constitutive model is needed to account for the change in gas volume fraction with reaction. For example, the decomposition gases nucleate in the polymer matrix to form defects, which grow and coalesce with reaction. Thermal expansion of the

polymer and nonideal vapor effects should also be considered. A constitutive law describing stress-strain behavior of reactive materials is beyond the scope of the current report. Instead, density changes are modeled empirically in the current report. For example, element death is assumed to cause the density to abruptly change from the initial foam density to the gas density, which spans the density for the open system. Thus, the foam density does not change for open system calculations. For closed systems, the density is not assumed to be constant as discussed further in Section 4.

3.4 Element Death Criterion

In CALORE, the solid fraction, m/m_o, is determined at each Gauss point and the average solid fraction is determined for each element. When the solid fraction within an element drops below a specified element death criterion, the element is removed from the computational domain and the surface boundary conditions are applied to the newly exposed elements, which exchange energy via radiation heat transport. This section discusses the selection of the element death criterion based on the calculated solid fraction within an element.

In CALORE, elements were removed from the computational domain when a specified criterion was reached. Removal of elements from the computational domain is referred to as "element death." A solid fraction death criterion, S_f^{death}, was used to control the elimination of elements during the computation. The solid fraction calculated within each element is checked every iteration to determine if the element should be removed from the computational domain. If the calculated solid fraction within an element falls below the death criterion, S_f^{death}, the element is removed from the computational domain.

In previous studies [5-7], the element death criterion was selected based on the measured onset of burnout. Burnout is defined as the solid mass fraction where most of the organic material has decomposed and the residue primarily consists of nonvolatile matter. The onset of burnout is the temperature at which burnout occurs. The onset point defines the transition from active mass loss to negligible mass loss near

the end of decomposition. The onset point is determined by the intersection of an initial tangent with the final tangent to the TGA mass loss profile. The temperature of the onset of burnout was determined for various experiments. In previous studies [5-7], the mean of the temperature corresponding to the onset of burnout was used with the mass loss model to define the death criterion.

The onset of burnout is a function of the degree that the decomposition products are confined, the system pressure, and the foam type. The onsets of burnout for each foam type (REF100, REF200, and REF300) were obtained at conditions where the predicted burnout (ultimate residue mass fraction) was the highest—totally confined decomposition. The predicted burnout for totally confined decomposition of REF100, REF200, and REF300 was 0.096, 0.164, and 0.132, respectively. The onsets to these final solid fractions were obtained using an initial tangent to the predicted mass loss curves. The death criterion for REF100, REF200, and REF300 was 0.126, 0.194, and 0.162, respectively. These *ad hoc* death criterions have significant uncertainty on the order of 0.030.

Substantial amounts of liquids are created during decomposition of REF100 at elevated temperatures. The onset of burnout for REF100 (0.126) is a reasonable choice for the element death criterion as long as liquids do not flow from the decomposition front. The element death criterion can also be used as an empirical method to mimic material relocation associated with liquid flow. In the current report, a solid fraction of 0.75 was used as the element death criterion to mimic flow from the decomposition front. At a solid fraction of 0.75, the viscosity may be low enough for gravity induced flow to be significant.

3.5 Grid Dependence

Element death is an *ad hoc* method of tracking the decomposition front and defining the dynamic radiation enclosure. More sophisticated methods, such as level set techniques [14], are being considered for future development of response models that form clean enclosures. One problem with element death is that the solution depends on the characteristic dimension of the element or grid as shown in Fig. 4.

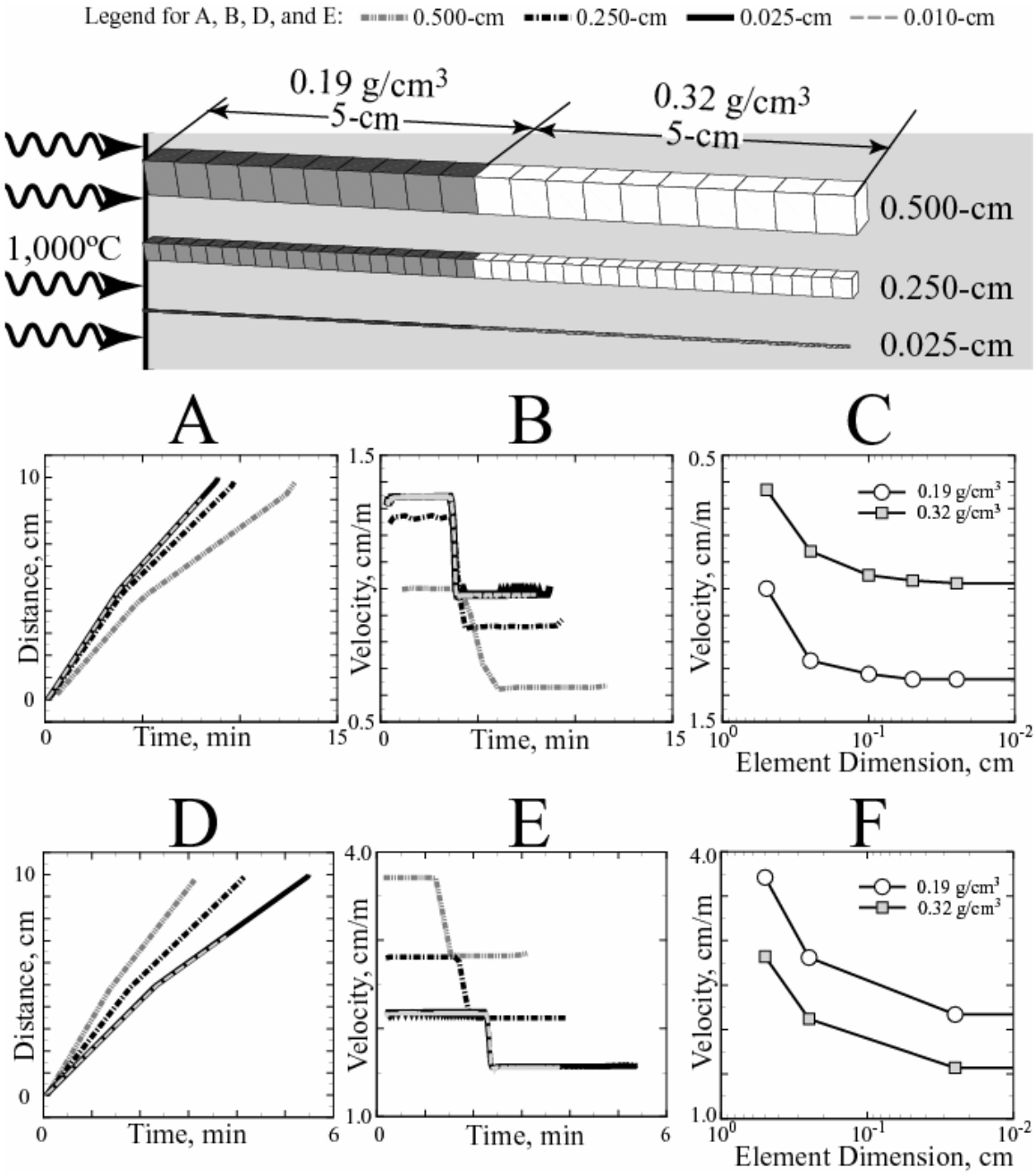

Fig. 4. 10-cm strand of foam constructed with various element dimensions with one end exposed to a 1,000ºC radiation temperature. The initial 5-cm of the strand has a density of 0.19-g/cm^3 (12-lb/ft^3) and the final 5-cm of the strand has a density of 0.32-g/cm^3 (20-lb/ft^3). A, B, and C show front location, front velocity, and grid dependency for SREF100 with $S_f^{death} = 0.126$, respectively. D, E, and F show front location, front velocity, and grid dependency for SREF100 with $S_f^{death} = 0.75$, respectively.

Figure 4 shows the calculated position and velocity of the decomposition front for a strand of foam exposed to a radiation temperature of 1,000ºC at various grid resolutions. The thermal conductivity used in the calculation was shown previously in Fig. 3.

As shown in Fig. 4, a single 10-cm strand of foam was constructed using two 5-cm strands at different densities—0.19 and 0.32 g/cm^3. The low-density end of the foam strand was exposed to a far-field radiation boundary temperature of 1,000ºC with a form factor of unity. The remaining surfaces of the foam strands were assumed insulated. In CALORE [2], the solid fraction, m/m_o, was determined at each Gauss point and the average solid fraction was determined for each element. When the solid fraction within an element dropped below a specified element death criterion, the element was removed from the computational domain and the surface boundary condition was applied to the newly exposed element – the exposed face of the foam strand exchanged energy via radiative heat transport to the far-field radiation temperature. Decomposition distances and velocities in Figs 4.A-4.C were calculated using an element death criterion of 0.126. Decomposition distances and velocities in Figs 4.E-4.F were calculated using an element death criterion of 0.75. Different death criterions were investigated since both are used to model foam response. The 0.75 death criterion is used to mimic flow as discussed previously in Section 3.3.

In Figs 4.A and 4.D, the ordinate is the distance that the decomposition front has traveled. The decomposition front separates the reacted region from the relatively unreacted foam. An element is considered part of the reacted region when the average solid fraction has dropped below the "death criterion," which was discussed in Section 3.3. The abscissa is the elapse time for element death. Zero time refers to the time when the strand is exposed to the radiation temperature. Thus, Figs. 4.A and 4.D are plots of the decomposition front location versus time. The decomposition front velocity is calculated as the derivative of the decomposition front location versus the elapsed time for element death and is shown in Figs. 4.B and 4.E. The decomposition front velocity is faster in the lower density foam than in the higher density foam.

Figure 4 shows the calculated decomposition front location and velocity determined using various element sizes ranging from 0.5-cm to 0.01-cm. As the size of the element decreased, grid independence was achieved. For both death criterions, grid independence was achieved when the size of the element was less than or equal to about 0.1-cm elements. Figures 4.C and 4.F show grid convergence for element death criterions of 0.126 and 0.75, respectively. Note that the front velocities *increased with smaller element size* when the death criterion was 0.126 until grid convergence was achieved at element sizes of about 0.1-cm. The opposite trend is noted in Fig. 4. E where a 0.75 death criterion was used—the front velocities *decreased when smaller elements* were used until grid convergence was obtained using 0.1-cm elements.

The difference between discretization convergences for the two different element death criterions is also illustrated in Fig. 5. In Fig. 5, the steady state front velocity is plotted as a function of both element size and the death criterion using a 0.13-g/cm^3 strand. For death criterions less than about 0.4, the steady state front velocity increases with smaller element sizes until grid independence is achieved. For this regime, grid dependency is related to the discrete removal of elements and the inheritance of the radiation

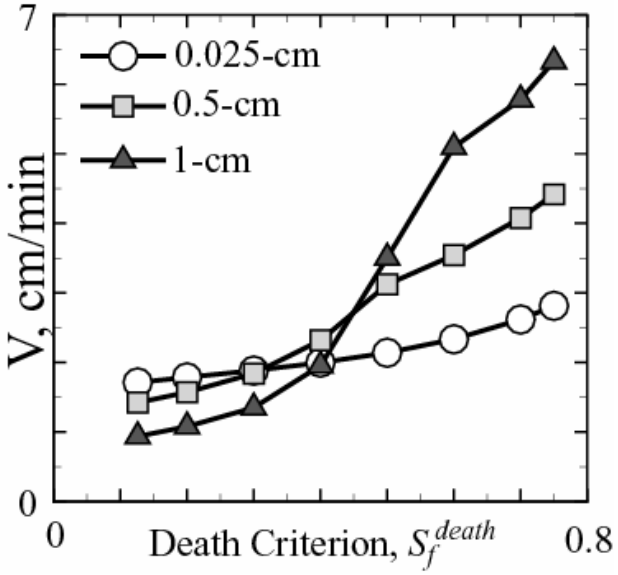

Fig. 5. Calculated strand velocities using 0.025-cm, 0. 5-cm, and 1-cm elements as a function of the element death criterion using SREF100 chemistry with 0.13-g/cm3 strands. This plot suggests that two discretization bias correction surfaces are needed: one to use when $S_f^{death} < 0.4$ when the large element velocities are too slow and a different surface to use when $S_f^{death} > 0.4$ when the large element velocities are too fast.

boundary condition on the newly exposed element. Since element death is delayed when larger elements are used, the reapplication of the radiation boundary condition to the next element is also delayed, making the decomposition front move more slowly, since radiation to a surface is a more efficient means of heat transfer than conduction through an element.

For element death criterions greater than about 0.4, the front velocity decreases when the element size is reduced until grid convergence is achieved at about 0.1-cm. This trend occurs when the death criterion is greater than about 0.4 since a significant amount of material is removed from the computational domain without kinetic-limited decomposition. When the death criterion is above 0.4, smaller elements allow more of the overall foam mass to participate in kinetic decomposition. Thus, larger element solutions, with element death criterions greater than about 0.4, give higher velocities than the grid independent solutions.

Since 0.1-cm elements are impractical for realistic three-dimensional system level calculations, a correction is needed to account for this bias associated with discretization. Also, two discretization bias correction schemes are needed to account for element death criterions that are less than about 0.4 and greater than 0.4. The discretization bias correction models should cause the front velocity to increase in velocity when the death criterion is less than about 0.4 and the element sizes are larger than 0.1-cm. Conversely, the discretization bias correction model should cause the front velocity to slow down when the death criterion is greater than about 0.4 and the element sizes are greater than 0.1-cm.

A discretization bias correction scheme was investigated for the SREF response model for use with elements larger than 0.1-cm. The SREF discretization bias correction model was found to be adequate for problems without encapsulated components. However for encapsulated components, the bias correction did not capture the correct thickness of residue remaining on the surface of the components, resulting in erroneous component temperatures. Thus, the discretization bias corrected solutions were not used in this report. Fully-grid-resolved calculations were performed for the current report using elements with characteristic dimensions on the order of 0.1-cm.

4. Dynamic Pressurization Model

The dynamic pressurization model for closed systems is based on a single element pressurization model discussed in reference [1]. The pressure at any state, *P*, is approximated using the ideal gas law as follows:

$$P = P^o \left(\frac{V_g^o}{V_g}\right)\left(\frac{n}{n^o}\right)\left(\frac{T}{T^o}\right), \tag{6}$$

where P^o, V_g^o, V_g, n, n^o, T, and T^o represent the initial system pressure, total initial gas volume in the enclosure, total gas moles in the enclosure, initial gas moles in the enclosure, average bulk temperature of the gases in the enclosure, and the initial bulk temperature of the gases in the enclosure, respectively. For multiprocessor simulations, the additional gas volume and gas moles need to be summed across processors. Summing across processors is accomplished in CALORE [2] with global variables, which are summed at every time step. The bulk temperature is also obtained using global variables by summing the volume weighted average temperature at all of the integration points within the foam material block.

In eqn (6), the gas volume in a sealed enclosure is the gas volume associated with the foam plus any excess gas volume that is not associated with the foam, referred to as excess volume, V_{excess}. Thus the gas volume is:

$$V_g = V_{excess} + \sum_{j=1}^{n} V_e^j \left(1 - \frac{S_{f,j}\rho_f^o}{\rho_p^o}\right), \tag{7}$$

where the summation is over *n* elements making up the foam material block. In eqn (7), V_e^j, $S_{f,j}$, ρ_f^o, and ρ_p^o refer to the volume of the j^{th} element, the reacted solid fraction within the j^{th} element, the initial foam density and the initial polymer density, respectively. The initial gas volume can be obtained by setting the reacted solid fraction to unity in eqn (7) as follows:

$$V_g = V_{excess} + \sum_{j=1}^{n} V_e^j \left(1 - \frac{\rho_f^o}{\rho_p^o}\right), \tag{8}$$

The number of moles is the initial moles of gas, n_o, plus the moles of gas generated via reactions:

$$n = n^o + \sum_{j=1}^{n} \frac{V_e^j \rho_f^o \left(1 - S_{f,j}\right)}{M_g^j}, \tag{9}$$

where M_g^j is the molecular weight of the reacted gas as determined with the SREF decomposition chemistry model. The initial moles of gas can be obtained using the ideal gas law as follows:

$$n^o = \frac{P^o V_g^o}{R T^o}. \tag{10}$$

The initial moles of gas do not depend on the molecular weight of the gases in the excess volume.

T_o is the initial temperature of the foam. The bulk temperature, T, was obtained using a volume weighted average temperature as follows:

$$T = \frac{\sum_{j=1}^{n} V_j T_j}{V_f}, \tag{11}$$

where T_j and V_j represent the temperature and volume of the j^{th} element, respectively. n is the number of elements in the enclosure. V_f is the total foam volume. Averaging over the elements in the enclosure should give reasonable results provided heat losses from the gas-phase are not significant.

For open systems, the pressure was assumed to be equal to the initial pressure. This pressure could be set using a pressure regulator and does not necessarily have to be set to ambient conditions. Also the density of the foam for open systems was assumed to be constant since a foam constitutive model was not available to determine the gas volume fraction. For closed systems, decomposition gases are not allowed to leave the system and the overall mass within the system is conserved. The dynamic foam density for closed systems is determined by summing the generated gas over all elements and redistributing the gas in the system evenly based on the volume fraction of the individual elements as follows:

$$\rho_{f,j} = \frac{\rho_f^o V_e^j - \left(1 - S_{f,j}\right)\rho_f^o V_e^j + \left(\sum_{j=1}^{n}\left(1 - S_{f,j}\right)\rho_f^o V_e^j\right)\frac{V_e^j}{V_f}}{V_e^j}, \tag{12}$$

which can be simplified to

$$\rho_f = \rho_f^o\left[S_{f,j} + \frac{\sum_{j=1}^{n}(1 - S_{f,j})V_e^j}{V_f}\right], \tag{13}$$

where V_f is the volume of the foam in the sealed enclosure. In summary, the input parameters for the pressurization model are ρ_f^o, ρ_p^o, V_f, V_{excess}, P^o, T^o, and R; the initialized parameters are V_g^o and n^o; the dynamic parameters are ρ_f, V_g, n, T, S_f, and M_g^j; and the parameters that require global sums for multiprocessor simulations are T, V_g, n, and ρ_f.

Intentionally left blank

5. Radiant Heat Experiments

The REF radiant heat experiments [3] were used to test the SREF response model for large-scale systems of interest. This initial comparison of model results using mean input parameters was not meant to validate the mean response or associated model uncertainty. Rather, the comparisons were used as an initial evaluation of the element death model and to give guidance in the selection of model parameters. This section presents the geometry of the various radiant heat experiments, the test matrix, the thermal boundary conditions, and the pressure boundary conditions for the pressure regulated experiments. Specific data on the thermal boundary conditions for each of the radiant heat experiments are included in the Appendix. Section 6 presents the SREF simulations of the radiant heat experiments. This section is meant to provide the geometry and boundary conditions for the simulations in Section 6. Details and evaluation of the radiant heat experiments will be documented by others.

5.1 Test Matrix

Table 2 describes the component-scale radiant heat experiments, which are segregated into four series of tests. More information regarding these experiments is given in reference [3] and the experiments are only summarized in this report. The interested reader should consult reference [3] for more information regarding the experimental program. The first and second series were run using REF100 and the third and fourth series were run using REF200. The first series is referred to as the AF series. The AF experiments were designed to look at ambient pressure decomposition with the applied heat flux parallel to the gravity vector. The acronym AF refers to “Able Foam” since REF100 was developed to replace the able foam used in older systems. The second series of tests were named the REF series to reflect the removability of the epoxy foam. The REF series were designed to investigate the effect of elevated pressure. For the REF series, the pressure in the experiments was regulated. The third series was named the “TUNA series” since the size of the confinement was about the size of a can of tuna. The TUNA series were designed to look at

Table 2 Component-scale radiant heat experiments with REF100 and REF200

	Descriptor[1]	Name	REF	Orientation	BC, ºC	P, atm	□, g/cm^3 (lb/ft^3)
Series 1 (AF) April-July 2001	A1top750	AF-1	100	TOP	750	0	0.128 (8)
	A2bot750	AF-2	100	BOT	750	0	0.128 (8)
	A4top750	AF-4	100	TOP	750	0	0.123 (7.7)
	A5bot750	AF-5	100	BOT	750	0	0.139 (8.7)
Series 2 (REF) March 2002	R6bot900-0	REF-6	100	BOT	900	0	0.122, 0.106 (7.6, 6.62)
	R8side750-0	REF-8	100	SIDE	750	0	0.120, 0.107 (7.5, 6.7)
	R11top750-2	REF-11	100	TOP	750	2	0.138 (8.6)
	R14bot750-2	REF-14	100	BOT	750	2	0.138 (8.6)
	R20top750-4	REF-20	100	TOP	750	4	0.112 (7)
	R22bot600-4	REF-22	100	BOT	600	4	0.139 (8.7)
	R23bot750-4	REF-23	100	BOT	750	4	0.131 (8.2)
Series 3 (TUNA) October 2002	T2top925-d20	TUNA-2	200	TOP	925	Dynamic	0.321 (20)
	T3top925-d8	TUNA-3	200	TOP	925	Dynamic	0.128 (8)
	T4top925-08	TUNA-4	200	TOP	925	BOT vent	0.128 (8)
	T5top925-020	TUNA-5	200	TOP	925	BOT vent	0.321 (20)
Series 4 (V) April 2003	V1top750	V1	200	TOP	750	0	0.159 (9.9)
	V2top750	V2	200	TOP	750	0	0.160 (10.0)
	V3top900	V3	200	TOP	900	0	0.165 (10.3)
	V4top900	V4	200	TOP	900	0	0.164 (10.3)
	V5bot750	V5	200	BOT	750	0	0.168 (10.5)
	V6bot750	V6	200	BOT	750	0	0.168 (10.5)
	V7bot900	V7	200	BOT	900	0	0.169 (10.5)
	V8bot900	V8	200	BOT	900	0	0.171 (10.7)
	V9side750	V9	200	SIDE	750	0	0.172 (10.7)
	V10side750	V10	200	SIDE	750	0	0.172 (10.8)
	V11side900	V11	200	SIDE	900	0	0.180 (11.3)
	V12side900	V12	200	SIDE	900	0	0.181 (11.3)
	V13top750	V13	200	TOP	750	0	0.159 (9.9)
	V14top750	V14	200	TOP	750	0	0.164 (10.2)
	V15side750	V15	200	SIDE	750	0	0.166 (10.3)
	V16side750	V16	200	SIDE	750	0	0.174 (10.9)

[1]Descriptors briefly describe each experiment. A, R, T, and V refer to the series AF, REF, TUNA, and V, repectively. Orientation of the heated surface with respect to the gravity vector is described by top, bot, and side. The top and bot thermal flux is parallel to the gravity vector, but in opposite directions. The side thermal flux is perpendicular to the gravity vecor. The numbers 600, 750, 900, and 925 refer to the control temperautre in the heated plate. For the "R" and "T" series experiments, an additional descriptor is used to describe the pressure in the experiment. If the last entry for these experiments is a number, then the identifier represents the nominal gauge pressure in atmosheres. If the last entry is a "d," then the pressure is dynamic, starting at zero gauge pressure. The last descriptor in the "T" experiments also gives the nominal foam density in lb/ft^3.

the effects of dynamic pressurization. The final series of test are referred to as the V series since the tests were used for validation. The "V" tests are referred to as the "MFER" test by Erickson et al. [4].

Each of the radiant heat experiments is described in detail in Table 2. The descriptor column identifies the particular experiment, the orientation of the experiment, the maximum temperature of the heated plate, the pressure, and the density of the experiment. For the REF series, the foam cylinders were sealed using a low-temperature-cure epoxy. Thermal expansion during the curing of the sealant epoxy for REF-6 and REF-8 caused the initial density of the foam to be less than the initial REF density. Both densities are listed for these experiments in Table 2.

5.2 Configurations

Figure 6.A shows the configuration for the AF and REF experimental series. Figure 6.B shows the confining metal skin with the approximate locations of the thermocouples. The REF experiments were similar to the AF experiments with the primary difference being the vent holes. Also, flame guards were not required in the REF series of experiments since decomposition gases were directed away from the experiments with stainless steel tube. The REF experiments were sealed at one end with a low-temperature-cure epoxy and the heated plate was welded to the confining sleeve, tubes were welded to the vent holes. The exhaust tubes were connected to a pressure regulator.

Figure 6.C and 6.D show the configuration for the TUNA and V experiments [4], respectively. The primary difference between the AF/REF experiments and the TUNA/V experimental configurations is the volume of foam. The AF/REF experiments used about 740cm^3 and 670 cm^3 of foam, respectively. The TUNA/V experiments used about 235cm^3 and 325 cm^3 of foam, respectively. Another major difference is that the V experiments contained a hollow and a solid encapsulated component. Locations of two of the thermocouples in the encapsulated component (T18 near the face of the solid component and T24 in the side of the hollow component) are shown in Fig. 6.D.

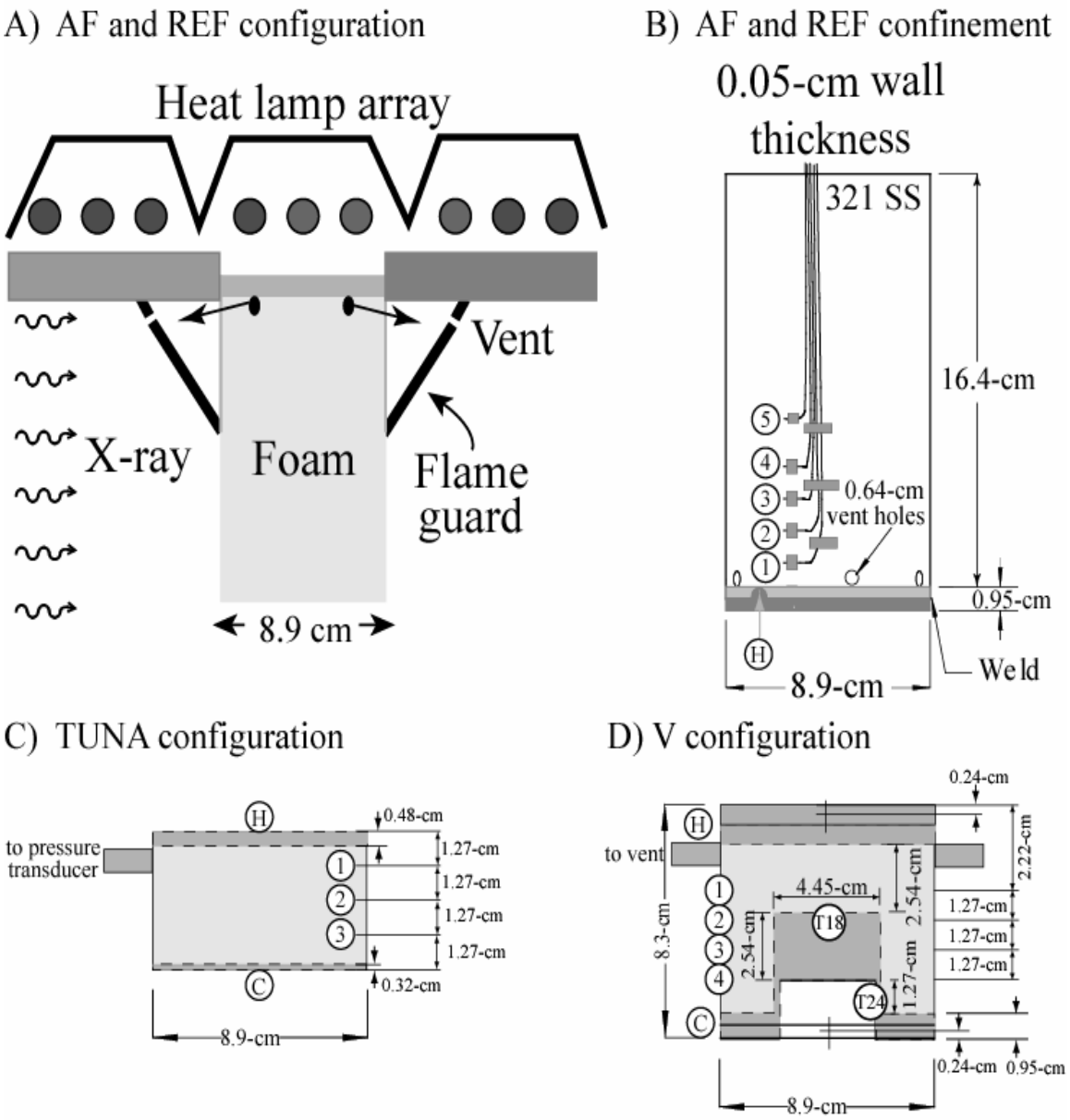

Fig. 6. Simple configuration of A) the AF and REF experimental series, B) AF and REF confinement can, C) TUNA experimental series, and D) the V experimental series. The numbers 1-5 represent the location of thermocouples on the confining can. The letters "C" and "H" represent the location of thermocouples in the end plates with "C" representing the "cold-side" and H representing the 'hot-side" of the experiment. T18 and T24 in D represent thermocouple locations in the embedded component. The REF series of experiments were similar to the AF series except that the cans were sealed and the vent holes were welded to 0.64-cm diameter tubes, which were connected to a pressure regulator. More information about the experiments can be found in [3,4].

The samples were heated by an array of quartz lamps as shown in Figs. 6.A. The samples were mounted to the middle of an insulation board that had an 8.9-cm hole, which exposed the samples to the heat lamps. The boundary temperatures were measured using thermocouples. Pressure was monitored in the REF and TUNA experiments with pressure transducers. The location of the thermocouples marked 1-5, "C", and "H" for the AF and REF series are shown in Fig. 6.B. The locations of the thermocouples for the TUNA series are marked with 1-3, "C", and "H" in Fig 6.C. The locations of the thermocouples for the V series are marked with a 1-4, "H", and, "C" in Figs. 6.D. The letter "H" represents the location of the control thermocouple on the "hot-side" of the heated-side of each experiment.

5.3 Temperature Boundary Conditions

The approximated temperature boundary conditions for the radiant heat experiments discussed in the current report are given in the Appendix. Detailed temperature boundary conditions are given in reference [4]. An example of the SREF boundary temperatures is given in Fig. 7.A for the T3top925-d8 experiment. In Fig. 7.A, the data from [3] is shown as thin black lines. The temperatures are somewhat noisy as shown in Fig. 7.A. The SREF boundary conditions were estimated from this data by selecting several points and linearly interpolating between these points. These estimated boundary temperatures are given in the Appendix for the experiments listed in Table 2.

Figure 7.B shows three radiographs [3] for experiment T3top925-d8. At 4 minutes, the linear front is near the heated surface located at the top of the can. The front becomes nonlinear as it moves down to about the middle of the can as shown in Fig. 7.B at 5 minutes. At 5 minutes, the front has become 3 dimensional and the fronts shape is difficult to estimate with the radiographs. The visual representation of the front is also uncertain due to the unknown orientation of the camera with the experiment. The location of the front was estimated by tracing the front using standard image processing tools. The traced image of the front was then transferred to the SREF prediction as shown in Fig. 7.B. The x-ray and vectorized front

were proportionally resized to be the same as the predictions. The radiographs were then deleted and the cartoon of the front was left on the prediction. The cartoons are 2D outlines of regions of higher density taken from radiographic images that integrate 3D information onto 2D image. The extrapolated front locations are highlighted with arrows. The SREF prediction in Fig. 7 was made using an element death criterion of 0.194 using SREF200 chemistry [1] and is discussed further in Section 6. Continuous gray-scale solid fraction contours are plotted with the legend given in Fig. 7. Only the author's interpretation of the radiograph front locations will be presented in the current document. Details regarding the radiographs will be documented by the experimentalists although some interpretation is given in [3].

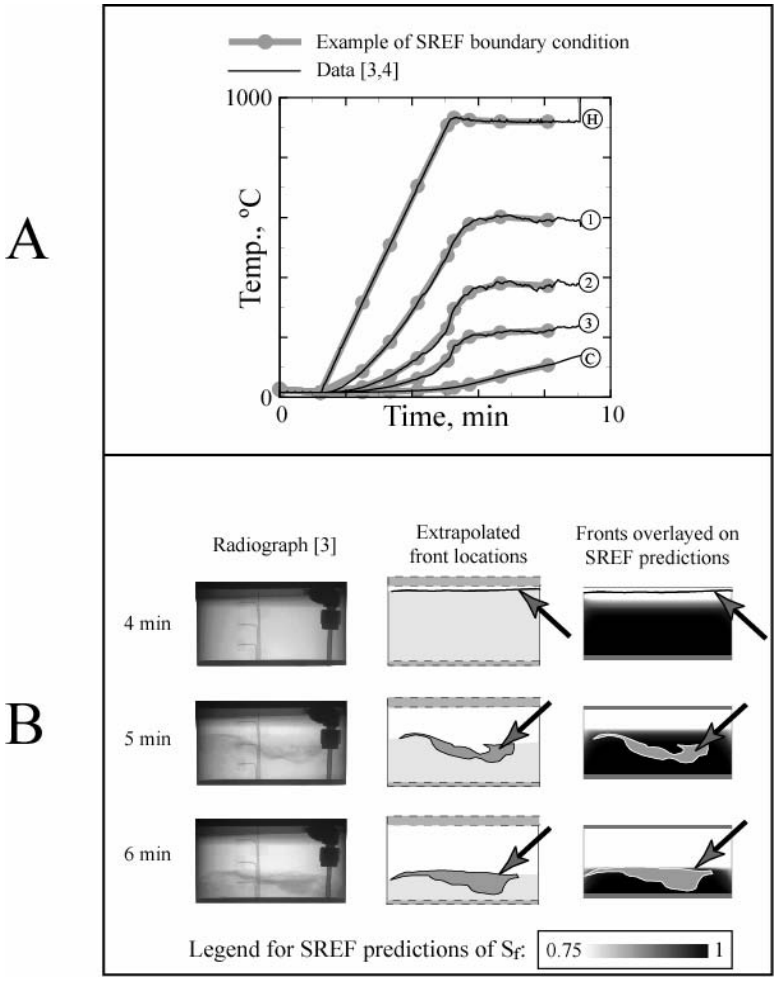

Fig. 7. Examples of A) SREF boundary temperatures and B) SREF front locations for experiment T3top925-d8. The locations of thermocouples H, 1, 2, 3, and C were given in Fig. 6.C. The measured temperatures in A are shown as thin black lines. The measured front locations can be seen as density variations in the radiograph. The imposed temperature boundary conditions for all of the tests are given in the Appendix.

6. SREF Simulations of the Radiant Heat Experiments

The simulations discussed in this section use SREF100 decomposition chemistry [1] for the AF and REF series of foam experiments and SREF200 decomposition chemistry [1] for the simulations of the TUNA and V series. The kinetic parameters given in Table 1 were used for the simulations. The element death criterions for the SREF100 ($S_f^{death} = 0.126$) and SREF200 ($S_f^{death} = 0.194$) series of foam were discussed previously in Section 3.3. These values of the death criterion were used when the foam was heated from the top and flow of liquefaction products was considered negligible.

The element death criterion was changed to 0.75 to *empirically* limit the accumulation of liquids at the decomposition front as discussed in Section 3.3 for experimental orientations that favor liquid flow (*e.g.* side-heated or bottom-heated configurations). Predictions for the AF and REF experiments in these orientations using an element death criterion of 0.75 were closer to fronts extrapolated from radiographs than predictions using element death criterions of 0.126. However, the front velocities were too high for the bottom and side-heated TUNA and V series when 0.75 was used since the amount of foam was not large enough to form significant quantities of decomposition liquids. Flow corrections were shown to be unnecessary when liquid accumulation was small.

6.1 AF series

Figure 8 shows foam response predicted using SREF100 chemistry [1] for A1top750, A2bot750, A4top750, and A5bot750. The 2D axisymmetric predictions of the solid fractions were made using 0.1-cm elements. The predictions are reflected about the vertical axis. The metal confinement is colored gray and legend for the solid fraction contours are the same as in Fig. 7 with the solid fractions below 0.75 being white and the 1.0 solid fractions being black. The lower bound, 0.75, was chosen since some of the simulations use a death criterion of 0.75. The plotted results look similar with the range of the scale changed from 0.126 to 1.0 since the decomposition fronts were typically thin. The arrows show the approximate location of the fronts that were interpolated from density variations in the radiographs.

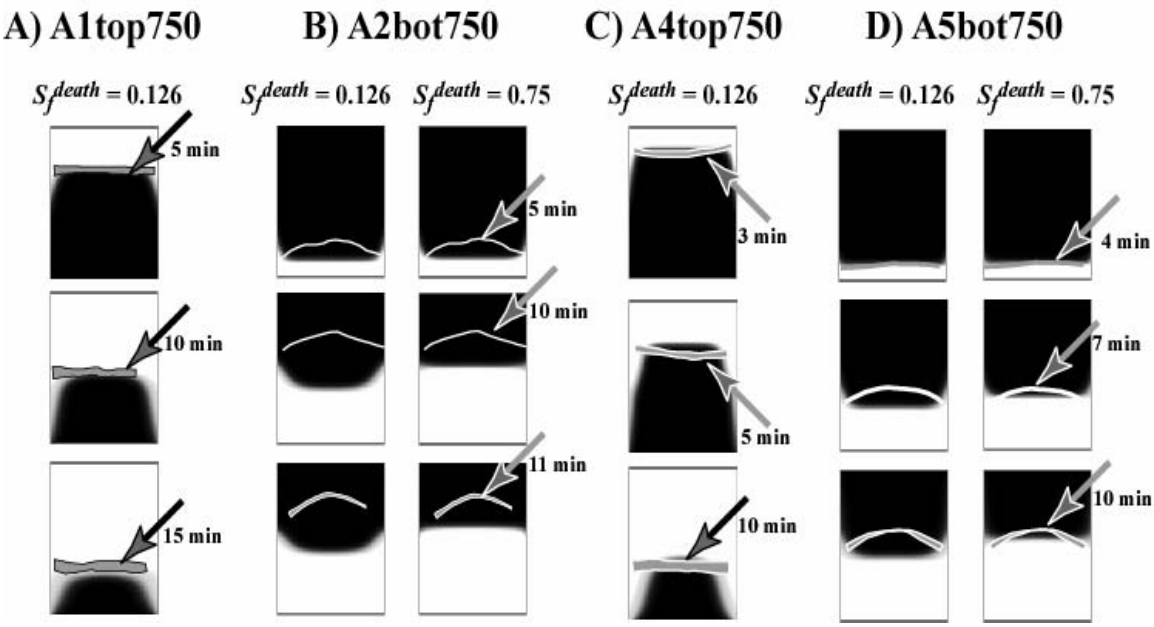

Fig. 8. Comparison between 2D axisymmetric SREF predictions and front locations interpolated from radiographs for experiments A) A1top750, B) A2bot750, C) A4top750, and D) A5bot750. The arrows show the approximate location of the fronts determined from the radiographs. The top-heated experiments used an element death criterion of 0.126. The bottom-heated experiments used an element death criterion of 0.126 and 0.75. The legend for the solid fraction contours are given in Fig. 7.

Liquid formation was apparent at the heated interface in the top-heated AF radiographs shown in Figs 8.A and 8.C. In these radiographs, the decomposition liquids remained at the heated interface since gravity induced flow paths were not available. The element death response model using an element death criterion of 0.126 was found sufficient to match the decomposition front locations for the top-heated AF experiments since flow effects were negligible. The element death response model appears to be a reasonable approximation for determining front location in the top heated experiments.

Liquid formation was also apparent at the heated interface in the bottom-heated AF radiographs [3]. In these radiographs, the decomposition liquids flowed from the center of the heated interface to the confinement walls with the liquid interface being thicker near the wall. The predicted front location using an element death criterion of 0.126 was not sufficient to match the front locations for the bottom-heated AF experiment as shown in Figs. 8.B and 8.D. The comparison between the predictions in Fig. 8.B and 8.D are

not as good as indicated since the solid fraction contours are only shown between 0.75 and 1.0. If the scale were changed to 0.126 to 1.0, then the mismatch between model and extrapolated front location would be even greater.

By changing the element death criterion to 0.75 for the bottom-heated experiments, the predicted front locations were closer to the front locations indicated in the radiographs. However, the experimental front curvature, which may have developed as the liquid flowed from the interface to the confinement walls, was not matched. The 0.126 element death criterion simulation of the bottom-heated AF experiments matches the observed front location during the early decomposition since significant liquids had not yet formed. As seen in Figs. 8.B and 8.D, the empirical flow model is not adequate to match the fronts as estimated from the radiographs. Liquid flow should be modeled as discussed further by Sun et al. [15].

6.2 REF series

Figure 9 shows comparisons between 2D axisymmetric SREF predictions and x-ray images [3] of R6bot900-0, R8side750-0, R11top750-2, R14bot750-2, R20top750-4, R22bot600-4, and R23bot750-4. The predictions are reflected about the vertical axis. The metal confinement is colored gray and legend for the solid fraction contours are the same as in Fig. 7 with the solid fractions below 0.75 being white and the solid fractions of 1.0 being black. The top-heated experiments used an element death criterion of 0.126. The bottom and side-heated experiments used an element death criterion of 0.75.

For the REF series of experiments, the flame guard was removed and each vent hole was connected by stainless steel tubing to a manifold that removed decomposition products from the vicinity of the heat lamps [3]. The presence of the exhaust tubes obscured the x-ray images near the heated plate and the uncertainty in the estimated location of the front using the radiographs is about 0.5 cm. For the R6bot900-0 experiment shown in Fig. 9.B, the foam expanded during curing of the low-temperature epoxy cure. Thus

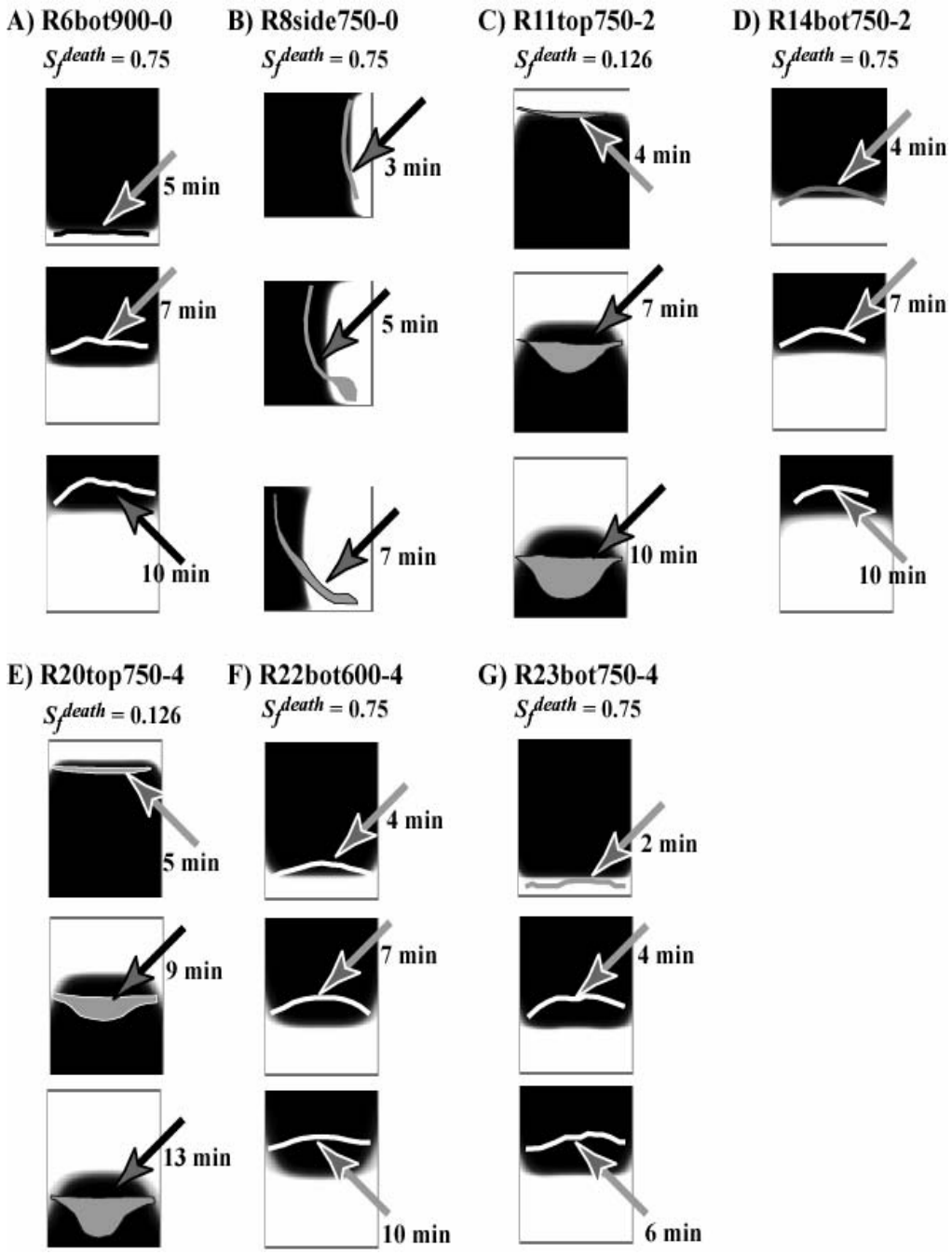

Fig. 9. Comparison between 2D axisymmetric SREF predictions and front locations interpolated from radiographs for experiments) R6bot900-0, B) R8side750-0, C) R11top750-2, D) R14bot750-2, E) R20top750-4, F) R22bot600-4, and G) R23bot750-4. The arrows show the approximate location of the fronts. The top-heated experiments used an element death criterion of 0.126. The bottom-heated experiments used an element death criterion of 0.75. The legend for the continuous solid fraction contours are given in Fig. 7.

the initial density of the foam is suspect and may account for differences in the predictions and measured front locations.

Figure 9.B shows predictions for the R8side750-0 experiment. The foam sample was heated in the side orientation with the heat flux from the lamps incident from the right. The vent on the underside of the can was capped. The other three vents were available to relieve gas pressure [3]. The thermal boundary conditions for the element death solution were obtained by averaging the thermocouples for all four quadrants. Notice that the fronts estimated from the radiographs show that more of the foam has regressed on the top of the can compared to the bottom of the can. This is not apparent in the 2D axisymmetric predictions. A 3D simulation was also run with 3D thermal boundary conditions that also showed this asymmetric front, but not as dramatically since the 3D simulation did not include a flow model. As indicated in the radiograph estimates, liquid decomposition products may have flowed under the influence of gravity and collected in the lower region of the container while the more volatile decomposition products left the system. This orientation effect was not as dramatic in the first 5 minutes of decomposition, which corresponds to about the volume of foam in the TUNA and V series of experiments.

Figures 9.C (R11top750-2) and 9.D (R14bot750-2) show the effect of orientation for decomposition with the pressure controlled at about 2.5 atm. In Fig. 9.C, the front behavior is significantly different when the gauge pressure is regulated to 2.5 atm when compared to unconfined decomposition shown previously in Fig. 8.A and 8.C for similar heating conditions. Rather than a simple liquid layer on a surface, the liquid seemed to permeate into the foam. Penetration of the liquid front into the foam may cause the apparent front velocity to increase. Hot liquid may promote heat transfer and liquefaction of the foam, which is not included in the foam response model. Similar behavior is shown when the gauge pressure is increased to 4.3 atm as shown in Fig. 9.E. This effect is not as dramatic when the orientation of the foam is changed so that the liquids flow from the heated interface as shown in Figs. 9.D, 9.F, and 9.G. The empirical flow model is not adequate to match the fronts estimated from the radiographs.

6.3 TUNA series

Comparison between 2D axisymmetric SREF predictions and front locations interpolated from radiographs for experiments T2top925-d20, T3top925-d8, T4top925-08, and T5top925-020 are shown in Fig. 10. Figures 10.A and 10.B show the decomposition of REF200 in a closed system. For these cases, the pressure was calculated based on the pressurization model discussed in Section 4 using two different decomposition rates. Only predictions determined with faster rates are shown in Fig. 10. The calculated and measured [3] pressures for these two experiments are shown in Fig. 11. The first set of calculations were based on using the faster rates obtained from unconfined TGA data. The second set of calculations were based on using the slower rates obtained from confined TGA data. The experimental data falls between the two predictions. However, the location of the decomposition fronts did not match the front locations estimated from radiographs when the slower rates were used. Both the predicted front and pressure determined using the faster rates were in better agreement with the data.

For the dynamic pressure experiments, the foam response model was only run until the container started to undergo significant deformation. The foam response model discussed in the current report does not consider quasi-static mechanics that are necessary to model the change in volume of the container associated with the pressure load created by the decomposition gases. However, the chemistry model is pressure dependent and feedback between the chemistry mechanism and pressurization model was included. Also channeling was evident in the radiographs as discussed in [3].

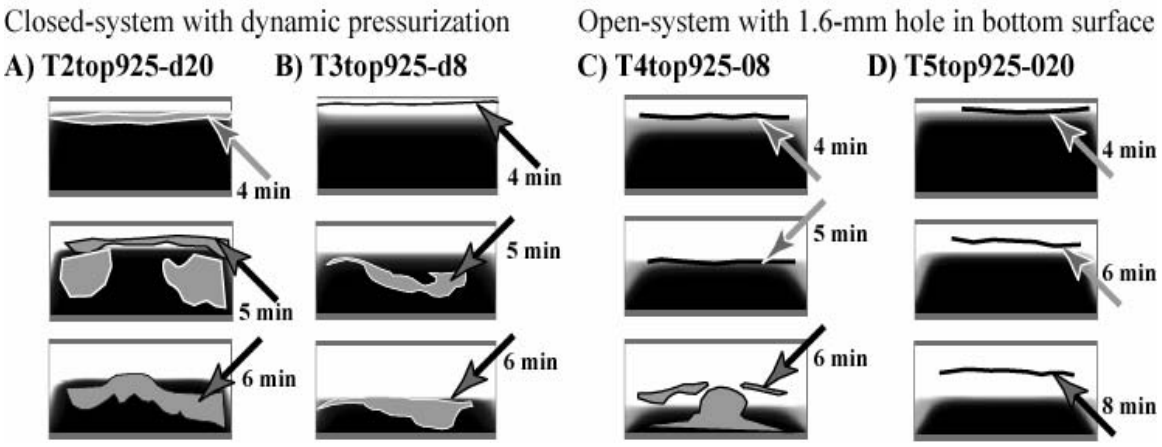

Fig. 10. Comparison between 2D axisymmetric SREF predictions and front locations interpolated for radiographs for experiments A) T2top925-d20, B) T3top925-d8, C) T4top925-08, and D) T5top925-020. The arrows show the approximate location of the fronts. All of these predictions used an element death criterion of 0.194. The legend for the continuous solid fraction contours are given in Fig. 7.

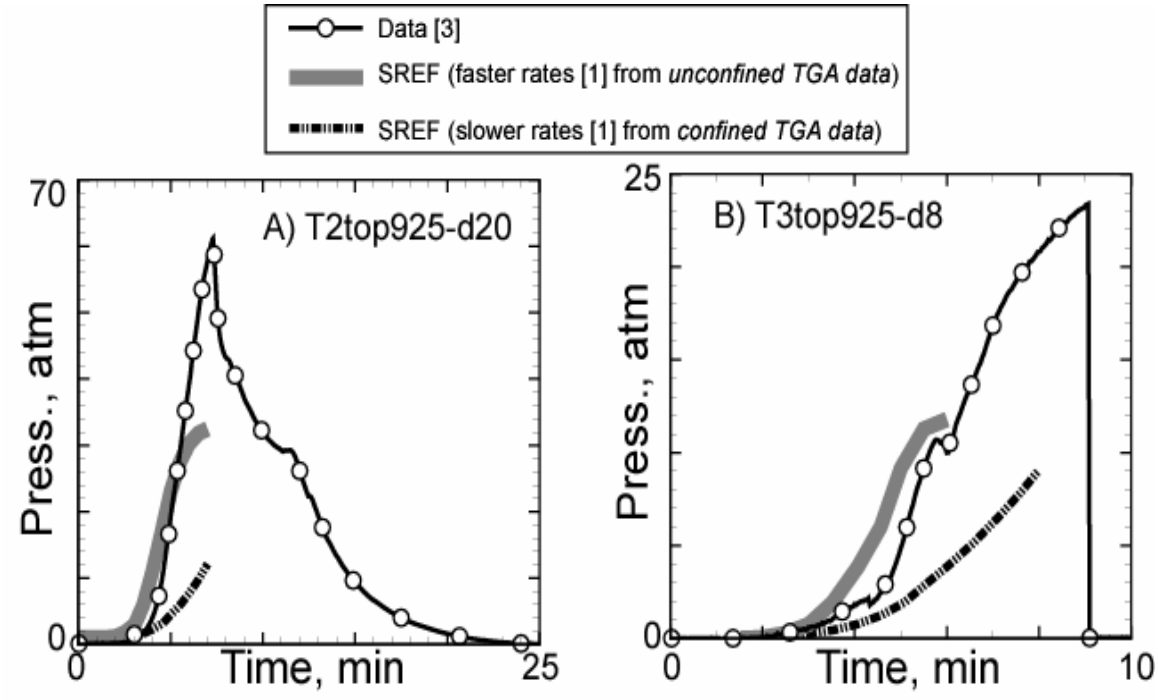

Fig. 11. Comparison between measured [3] and predicted pressurization of A) T2top925-d20 and B) T3top925-d8. The predictions were made using an element death criterion of 0.194.

Figures 10.A and 10.B show the effect of density on totally confined decomposition with dynamic pressurization of the confinement. The interpolated fronts in Figs. 10.A and 10.B show some asymmetry as the three-dimensional regression of the foam occurs. The pressure in the experiment with the higher density foam (T2top925-d20 in Fig. 10.A) got as high as 60 atm before the weld around the pressure tap failed, and the container gradually vented [3]. The pressure in the lower density foam (T3top925-d8 in Fig. 17.B) got as high as 25 atm before the container failed violently [3].

The experiments shown in Fig. 10.C and 10.D were performed with a small hole in the bottom plate opposite from the heated surface. Erickson et al. [3] observed an erosive channel in T5top925-020 that occurred between 3 and 4 minutes. The release of substantial liquid from the experiment through the bottom plate may explain the differences between the SREF predictions and the interpolated front location shown in Fig. 10.D. The hot liquids can induce additional liquefaction or become a source of liquid accumulation as the liquid exits the vent hole in the bottom of the experiment. These experiments show that flow can proceed by gravity as well as by pressure gradients caused by small vents or leaks in systems of interest.

6.4 V series

Comparison between the foam response predictions using SREF200 chemistry [1] and front locations interpolated from radiographs for the V series of experiments heated to 750ºC and 900ºC at various orientations are shown in Fig. 12. In Fig. 12, parts A/D, B/E, and C/F show top-heated, side heated, and bottom heated experiments, respectively. The top and side-heated experiments at 750ºC were repeated 4 times each. The remaining V experiments were repeated once. Temperature boundary conditions are given in the Appendix. The density of the foam was given in Table 2.

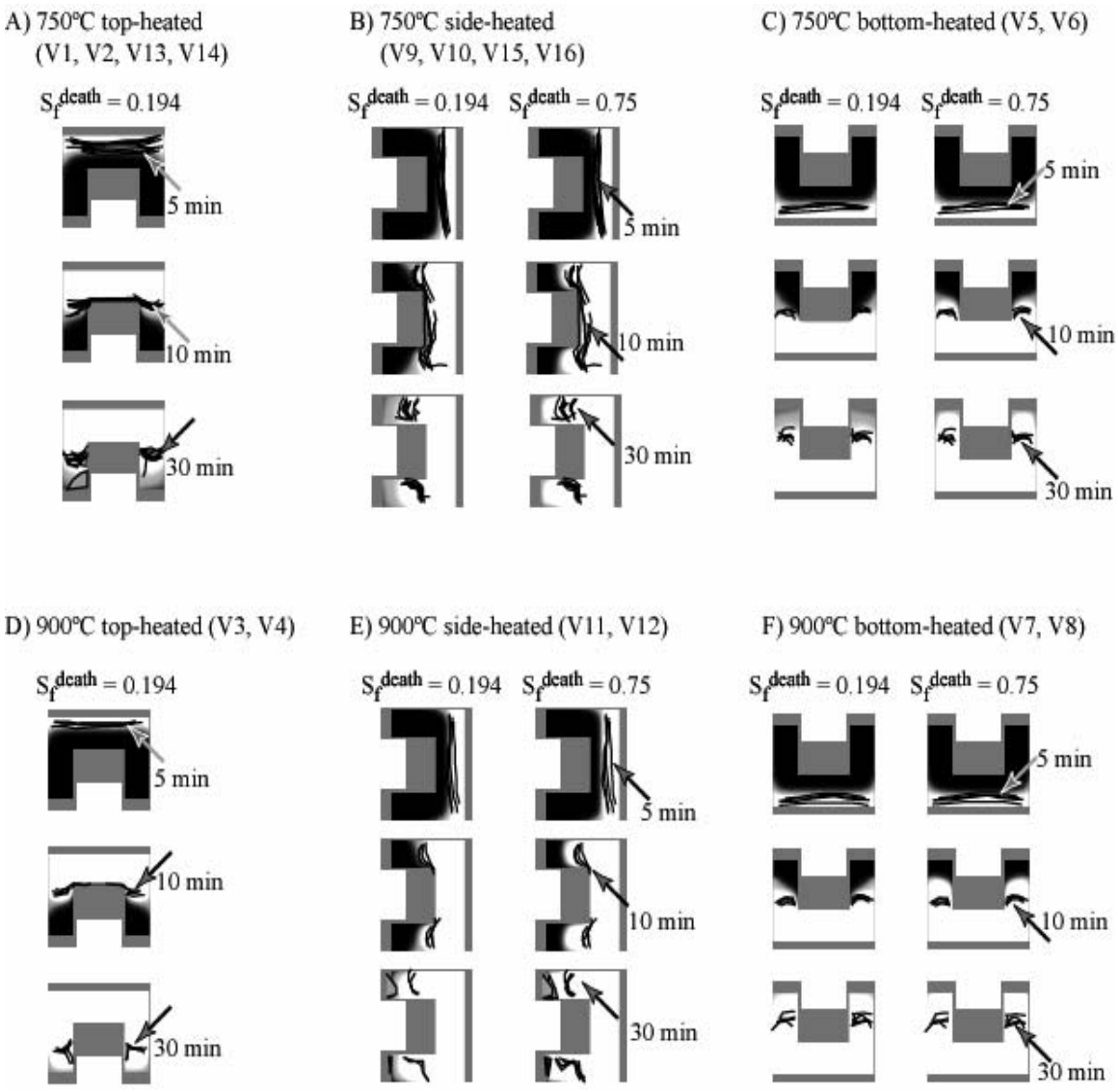

Fig. 12. Comparison between 2D axisymmetric SREF predictions and front locations interpolated from radiographs for V experiments heated to 750ºC from the A) top, B) side, and C) bottom as well as experiments heated to 900ºC from the D) top, E) side, and F) bottom. The legend for the predicted solid fraction contours was given in Fig. 7.

Two x-ray cameras separated by an angle of about 60 degrees were used for the V series of experiments [3]. From the radiographs, the decomposition front could be seen as density variations. The front locations were interpolated from the radiographs using standard image processing software. The front locations were traced on the radiograph using a pen tool. The traced font and the radiographs were grouped and made to match the SREF simulation by using a constrained resize function and the radiograph was scaled proportionately. The radiographs with the traced fronts were then placed on the SREF predictions and the radiographs were deleted leaving the traced front on the SREF prediction. In Fig. 12.A and 12.B, eight traced fronts are shown for the four replicate experiments since two radiographs were taken at each time. Four traced fronts are shown on the remainder of the images in Fig. 12.

Figure 12.A shows a comparison between the element death response model and front locations interpolated from radiographs for the top heated V experiments with the set temperature at 750ºC. At 30 minutes, the fronts interpolated from the radiographs show liquid near the hollow end of the component. This only occurred for experiment V12. Liquid decomposition products may have migrated down the side of the component and accumulated at the bottom of the confinement can. In Fig. 12.B and 12.C, the element death model was used with a solid fraction based element death criterion of both 0.194 and 0.75. The 0.75 element criterion represents an empirical flow model that causes the front to move more rapidly to account for liquid flow from the heated interface. Since significant amounts of liquids are not formed in these experiments, the empirical flow model caused the fronts to move faster than indicated in the radiographs. The predicted front velocity using an element death criterion of 0.75 was too fast especially as the foam decomposed below the embedded component. In this region, liquid movement was restricted, and the flow correction may have been too aggressive. Similar conclusions can be made for the bottom heated experiments shown in Fig. 12.E and 12.F.

Substantial residue remained in the experiment at the end of the experiment. The element death model does not retain the residues in the enclosure and predicts that more of the surface of the encapsulated

component is exposed to the hot boundary conditions than in the experiment. For any given experiment, about 20% by mass of the original foam will remain in the enclosure, unless the residue exits the system. All of the experiments show that residue remains near the hollow side of the encapsulated component. The element death response model does not retain residue--residue is removed when elements die. In fact, the element response model predicts that no foam residue is left on the surface of the embedded component, which is contrary to postmortem experimental observation (actual *in situ* response is unknown). The consequence of removing excess residue was that a clean embedded component was exposed at late times as observed in all of the experiments at 30 minutes in Fig. 12. The measured temperatures of the components at late times were not as hot as the predictions since the components were covered with residue.

Figure 13 shows the predicted temperatures at two locations within the embedded component in the V experiments. The two locations are indicated in Fig. 6.D labeled T18 and T24. These designators are the thermocouple numbers used in the actual experiments. Only T18 and T24 temperatures are shown since these two temperatures show the greatest variation in the component temperatures. The temperature at T18 is dominated by foam decomposition since it is the temperature at the middle of the component, away from the walls and faces the heated surface. Thermocouple T24 is in direct contact to the colder plate and the temperature response at this location is not dominated by the foam response. However, the predicted temperature at T18 is dominated by the foam response. In Fig. 13, the SREF model predicts that the surface of the component facing the heated plate is completely exposed to the hot skin temperatures at about 33 minutes for the experiments at 750ºC and at about 25-35 minutes for the experiments at 900ºC. In Fig. 13, arrows show the time when the last element was removed from the face of the component facing the hot surface. A similar abrupt change in the temperature at T18 was not observed in the experiments.

In Fig. 13, the plots A, B, and C are for the experiments run at 750ºC. The plots D, E, and F are for the experiments run at 900ºC. The top figures (Fig. 13.A and 13.D) are for the top-heated experiments

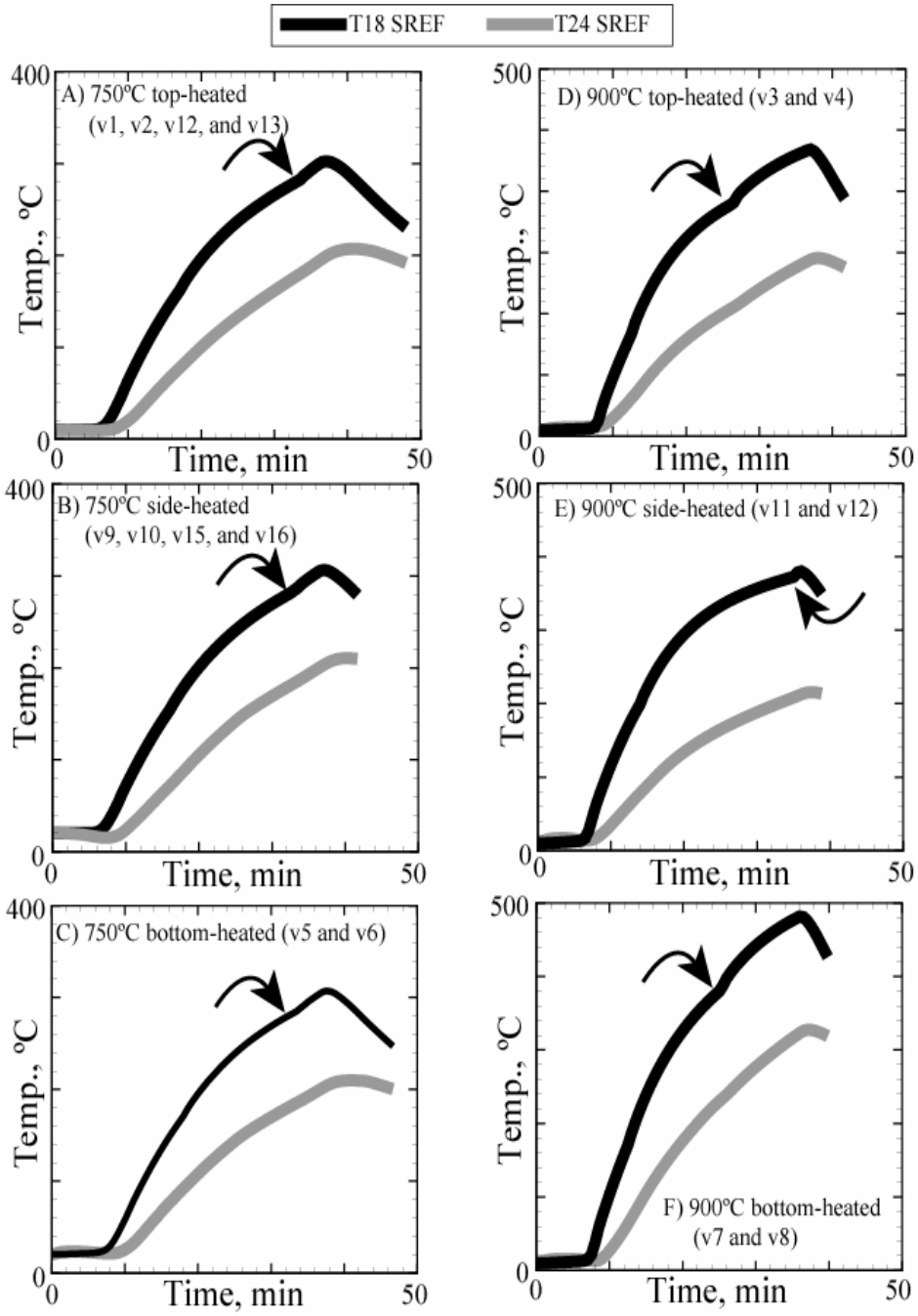

Fig. 13. Predictions of encapsulated components temperatures in the V series of experiments. The location of the temperatures labeled T18 and T24 is given in Fig. 6.D. The predictions of temperatures at T24 were generally in agreement with the experimental data. However, the predictions of the temperatures at T18 were generally too high. Arrows show the time when the last element was removed from the face of the component facing the hot surface.

and the middle plots (Fig. 13.B and 13.E) are for the side-heated experiments. The bottom-heated experiments are the bottom plots in Figs. 13.C and 13.F. In Fig. 13, the thick black lines represent the model prediction of the temperature that is located at the node nearest the T18 thermocouple. The thick gray lines represent the model prediction of the temperature located at the node nearest the T24 thermocouple.

The predicted temperature at T24 is within the scatter of the measured data indicating that the conduction-dominated temperature at this location is predicted accurately. However, the predicted temperature at T18 is about 20ºC too high when compared to the measured temperatures for the experiments run at 750ºC. The difference between the predictions and measurement is about 100ºC for the experiments run at 900ºC at T18. This bias between the prediction and measurements indicates missing physics or bad assumptions in the response model. The predicted and measured component temperatures were close during the first 10 minutes. After 10 minutes, the predictions were always higher than the measurements for T18. The measured temperatures at T18 were always in between the predicted temperatures at T28 and T18. The inability of the model to predict the component face temperature may be related to the surface properties of the component.

Erickson et al. [3] shows a postmortem radiograph of the residue left in one of the TUNA experiments showing a complicated layered structure of thin layers of partially decomposed foam (residue) separated by large void regions on the order of 1-cm. The postmortem radiographs may not adequately represent the state of the degraded foam during the experiments. However, a complex structure of surfaces may exist during the decomposition. These surfaces may impede radiation transport and limit heat transfer to the embedded components. A “dirty-enclosure” may not be modeled adequately using an element death technique. A more appropriate response model may be an effective conductivity model. More information regarding effective conductivity models can be found in the review article by Collishaw and Evans [16].

Intentionally left blank

7. Summary and Conclusions

This report describes a foam response model based on element death that has been implemented into the finite element thermal/chemistry code, CALORE [2]. The response model uses a chemistry model [1] that is based upon the chemical structure of rigid, closed-cell removable epoxy foams. The chemistry model describes the mass loss associated with irreversible thermal degradation along with the evolution of the condensed and gas-phase molecular weight distributions. The response model describes the propagation of a decomposition front resulting from exposure of the foam to abnormal thermal environments. The response model also describes pressurization in closed systems.

The element death response model relies on dynamic radiation enclosures to propagate the decomposition front. The gases within the enclosure were assumed to be nonparticipating transparent gases. In the element death model, elements are removed from the computational domain when the calculated solid fraction drops below a specified element death criterion. The element death criterion is the value of the solid fraction that corresponds to the onset of burnout, which occurs when most of the organic material has decomposed and the residue consists of nonvolatile material. The radiation surface boundary conditions are applied to the newly exposed elements, which exchange energy with the hot surrounding walls via radiation. The element death model utilizes the solid fraction that is predicted with the chemistry model [1]. For confined systems, the element death model also uses the predicted gas molecular weight to predict pressurization. The element death response model removes the entire element even though as much as 20% by mass of the foam forms solid residues that do not vaporize. Complete element removal that does not account for nonvolatile residue formation biases the prediction of temperature in embedded components. The predicted temperatures are higher than the measured temperatures.

The element death criterion was used to empirically model the effect of fluid flow. In the current report, a solid fraction value of 0.75 was used to mimic material relocation associated with liquid flow. The element death criterion of 0.75 corresponds to the solid fraction where the REF polymer is expected to

be a low viscosity liquid. The empirical flow model gave reasonable predictions provided the amount of foam liquid formation was substantial. However, the shape of the decomposition front was not predicted adequately.

Removing elements with an element death criterion of 0.75 caused the decomposition fronts to move faster and the front thickness to decrease when compared to simulations with death criterions near 0.2. An empirical element death criterion of 0.75 was found to be sufficient for the bottom- and side-heated AF and REF experiments where the amount of foam was large [3]. For systems with smaller amounts of foam such as in the TUNA and V radiant heat experiments [3] an element death criterion of 0.75 caused the decomposition fronts to propagate too fast. In fact, the predicted fronts quickly decomposed all of the foam in the V series of experiments and exposed the previously embedded components to the hot confinement walls. This caused additional uncertainty since the emissivity of the components became important. Using an empirical flow model (setting the death criterion to 0.75) is not recommended for simulations where the amount of foam is small, such as in the TUNA and V radiant heat experiments [3]. Furthermore, the empirical flow model does not predict the correct shape of the decomposition front. A more rigorous model that accounts for liquid flow such as discussed by Sun et al. [15] is needed to predict effects of liquefaction.

Four series of radiant heat experiments were simulated with the element death response model – 1) AF series, 2) REF series, 3) TUNA series, and 4) V series. The AF and REF series were run using REF100 and the TUNA and V series were run using REF200 foam. The AF and REF series used foam samples that were approximately 740-cm^3 and the TUNA and V series used approximately 235-cm^3 of foam. The larger volume samples produced more liquids and had significant orientation effects. Orientation effects were not as obvious in the TUNA and V series, perhaps due to the smaller volumes of foam.

Only the orientation was varied for the AF series of experiments. The set temperature of the heated plate was kept constant at 750ºC. For the top heated experiments, the flow correction was not

needed to match the observed decomposition front in the x-ray images using the element death model. For the bottom-heated experiments, the flow correction using a 0.75 element death criterion was necessary to match the observed decomposition front in the x-ray images.

The REF series of experiments were similar to the AF experiments except that different set temperatures, orientations, and pressures were investigated. The pressures in the REF experiments were maintained with a pressure regulator. At elevated pressure, the element death simulations, using the flow correction model for the bottom-heated and side-heated experiments, matched the front locations observed in the x-ray images. However, for the top-heated experiments, the predicted front velocities were too slow when the set pressure was either 2.5 or 4.3 atmospheres. For these cases, the liquid at the front may have permeated into the relatively unreacted foam and promoted heat transfer and possible liquefaction.

Orientation effects were not pronounced in the TUNA and V series of experiments in comparison to the AF and REF experiments. The insensitivity to orientation is probably related to the amount of foam in these experiments, which is roughly one-third of the foam in the AF and REF experiments. The TUNA experiments were all performed with a set temperature of 925ºC. Two of the TUNA experiments were performed with a small hole in the confinement on the end opposite from the heated surface. This hole caused unusual flow of liquids that was not modeled. Pressure rise caused by decomposition was modeled for two of the TUNA experiments. Two different rate models were used to simulate the pressure in the TUNA experiments—1) faster rates associated with unconfined TGA data and 2) slower rates associated with confined TGA data. The faster rate simulations of pressure rise were closer to the measured pressure rise using a pressure transducer. The measured pressure was always between the two simulations performed with both the faster and slower rates. However, the simulations performed with the faster rates associated with the unconfined TGA results were closest to the measurements, even though the experiments were totally confined. These results imply that the confinement effect measured in the small-scale TGA experiments do not scale to the larger radiant heat experiments.

The V series of experiments included embedded components. The ultimate goal of the foam response model was to provide a means of predicting accurate temperatures of embedded components. In the V series of experiments several thermocouples were used to access the response models. The finite element model easily predicted component temperatures at locations near the walls of the confinement since conduction was the primary mode of heat transfer at these locations. However, the finite element model required a more accurate description of the foam response to predict the temperature of the component face that was completely encapsulated with foam. The temperatures predicted with the element death model were 20-100ºC higher than the measured component temperatures. Possible reasons for higher predicted component temperature are 1) complete element removal without accounting for nonvolatile residue and 2) unknown component surface properties associated with the decomposing foam.

In summary, a response model has been developed for systems analysis based on the SREF decomposition chemistry model [1]. The response model is based on element death and uses dynamic radiation enclosures. This model is computationally expensive since viewfactors need to be recomputed whenever an element is removed from the computational domain. The element death model also assumes that the enclosure is filled with transparent, non-participating gases. The element death model may be required when significant amounts of foam are decomposed and heating conditions are such that fragile foam residues collapse and create transparent enclosures. However, component response may be dominated by these nonvolatile residues. Furthermore, thin layers of partially decomposed foam have been observed that appear to be a network of absorbing and re-radiating surfaces [3]. For these systems, an effective thermal conductivity model based on bubble nucleation, growth, and coalescence is recommended.

Appendix

The appendix contains the FORTRAN data statements used to specify the boundary conditions for each of the REF radiant heat experiments discussed in this report. The temperatures for the TUNA and V series were fit to the measured temperatures in reference [4].

Boundary Conditions:

A1top750

```
C z distance from bottom plate TC to CUP TC's
      data z/ 0.0, 0.48, 1.11, 2.38, 3.65, 4.92, 6.83,16.51/
C ts time in s
      data ts/ 0., 25.6, 40.8, 97.0, 104.4, 113.3, 116.2, 145.6, 164.4,
     & 217.9, 222.1, 240.3, 244.4, 268.2, 295.8, 303.1, 319.2, 335.2,
     & 338.2, 362.0, 378.2, 405.9, 429.4, 476.8, 518.7, 561.9, 629.6,
     & 741.0, 850.8, 980.1, 1112.8, 1196.3, 1291.3, 1384.9, 1487.4,
     & 1591.7, 1711.8/
C t0 thermocouple 0 (bottom plate thermal couple)
      data t0/ 300.0, 294.5, 322.8, 954.7, 1005.3, 1020.6, 1021.2,
     & 1010.9, 1008.1, 1009.0, 1009.3, 1010.1, 1010.3, 1011.1, 1012.4,
     & 1012.6, 1012.2, 1012.6, 1012.5, 1012.6, 1013.3, 1015.0, 1015.4,
     & 1015.0, 1015.8, 1016.2, 1015.4, 1014.9, 1015.0, 1014.1, 1013.1,
     & 910.7, 824.4, 759.9, 704.5, 659.7, 617.1/
C t1 thermocouple 1
      data t1/ 300.0, 295.4, 302.4, 586.6, 641.8, 690.0, 702.0, 770.2,
     & 789.5, 827.3, 852.0, 839.5, 839.1, 843.7, 847.6, 894.6, 881.1,
     & 880.4, 893.7, 884.0, 875.3, 874.5, 877.6, 926.2, 916.4, 898.6,
     & 886.8, 878.8, 884.3, 878.8, 875.5, 821.6, 754.4, 700.1, 651.9,
     & 612.0, 573.6/
C t2 thermocouple 2
      data t2/ 300.0, 295.5, 298.3, 453.0, 494.9, 536.6, 548.2, 633.5,
     & 664.6, 731.5, 766.0, 756.8, 756.1, 762.4, 768.8, 825.2, 824.9,
     & 828.6, 844.9, 830.5, 814.3, 810.4, 814.4, 886.4, 880.4, 848.1,
     & 833.0, 824.3, 828.4, 825.5, 822.2, 781.0, 720.2, 669.2, 623.9,
     & 586.0, 549.4/
C t3 thermocouple 3
      data t3/ 300.0, 295.8, 296.8, 344.7, 363.4, 387.6, 394.8, 454.2,
     & 484.9, 563.9, 608.3, 619.1, 620.5, 637.1, 652.2, 709.5, 750.0,
     & 754.6, 781.9, 751.7, 732.6, 726.8, 731.2, 833.0, 841.8, 785.3,
     & 765.4, 755.8, 759.2, 757.3, 754.3, 726.3, 673.3, 626.3, 584.2,
     & 549.0, 515.0/
C t4 thermocouple 4
      data t4/ 300.0, 296.1, 296.8, 315.6, 323.7, 334.5, 337.8, 371.2,
     & 393.9, 449.0, 476.0, 500.0, 499.9, 513.6, 532.4, 562.0, 642.3,
     & 653.2, 661.6, 664.3, 652.4, 650.4, 658.1, 754.9, 829.6, 734.0,
     & 713.4, 704.5, 709.9, 709.2, 707.0, 686.7, 640.2, 596.0, 556.6,
     & 523.1, 491.0/
C t5 thermocouple 5
      data t5/ 300.0, 296.3, 296.8, 307.9, 311.5, 317.6, 319.0, 335.3,
     & 349.5, 387.3, 393.6, 422.2, 423.3, 435.6, 451.1, 462.9, 499.5,
     & 527.9, 531.7, 555.0, 553.6, 557.3, 566.1, 633.7, 680.5, 668.0,
     & 654.2, 651.8, 666.0, 669.3, 668.8, 655.0, 613.9, 572.2, 535.4,
     & 503.1, 472.4/
```

```
C t6 thermocouple 6
      data t6/ 300.0, 296.7, 297.4, 311.2, 312.4, 315.3, 314.9, 318.6,
     & 324.2, 338.6, 339.6, 352.1, 353.2, 363.7, 370.8, 372.3, 383.7,
     & 398.4, 397.1, 412.7, 423.3, 430.7, 440.2, 456.3, 484.3, 505.9,
     & 497.5, 499.7, 533.8, 546.3, 562.9, 567.2, 542.0, 513.0, 485.4,
     & 457.6, 432.1/
C t7 thermocouple 7 (Assumed temperature at the top of the cup)
      data t7/ 300., 300., 300., 300., 300., 300., 300., 300., 300.,
     & 300., 300., 300., 300., 300., 300., 300., 300., 300., 300.,
     & 300., 300., 300., 300., 300., 300., 300., 300., 300., 300.,
     & 300., 300., 300., 300., 300., 300., 300., 300./
```

A2bot750

```
C z distance from bottom plate TC to CUP TC's
      data z/ 0.0, 0.48, 1.11, 2.38, 3.65, 4.92, 6.83,16.51/
C ts time in s
      data ts/ 0.000, 154.8, 174.8, 184.8, 209.8, 239.8, 254.8, 279.8,
     & 304.8, 344.8, 404.8, 499.8, 549.8, 599.8, 689.8, 754.8, 889.8,
     & 989.8, 1189.8, 1384.8/
C t0 thermocouple 0 (bottom plate thermal couple)
      data t0/ 300.0, 296.4, 296.4, 321.8, 605.8, 946.4, 998.1, 1007.8,
     & 1009.8, 1010.7, 1012.3, 1012.9, 1014.5, 1015.0, 1014.9, 947.9,
     & 828.9, 765.1, 672.4, 609.4/
C t1 thermocouple 1
      data t1/ 300.0, 298.0, 298.0, 300.1, 391.9, 611.1, 699.8, 769.2,
     & 801.9, 829.3, 844.6, 861.0, 866.8, 868.7, 870.6, 841.8, 757.9,
     & 701.7, 618.2, 565.2/
C t2 thermocouple 2
      data t2/ 300.0, 298.9, 298.9, 299.3, 332.5, 468.7, 550.6, 638.4,
     & 685.9, 728.4, 751.2, 768.6, 776.0, 775.9, 775.9, 761.2, 705.5,
     & 653.8, 578.6, 533.8/
C t3 thermocouple 3
      data t3/ 300.0, 300.1, 300.1, 300.5, 305.2, 344.2, 387.5, 457.8,
     & 513.7, 586.2, 641.2, 675.9, 687.5, 690.9, 686.6, 681.1, 650.9,
     & 602.0, 534.5, 496.1/
C t4 thermocouple 4
      data t4/ 300.0, 301.0, 301.2, 301.5, 303.0, 316.0, 333.2, 372.4,
     & 421.3, 481.4, 542.7, 612.3, 630.8, 646.3, 646.2, 644.0, 620.2,
     & 573.8, 509.8, 473.1/
C t5 thermocouple 5
      data t5/ 300.0, 300.0, 300.0, 300.0, 300.0, 300.0, 300.0, 301.0,
     & 307.0, 321.0, 346.0, 485.0, 517.0, 557.0, 565.0, 570.0, 563.5,
     & 537.0, 480.0, 447.0/
C t6 thermocouple 6
      data t6/ 300.0, 300.0, 300.0, 300.0, 300.0, 300.0, 300.0, 300.0,
     & 300.0, 300.0, 300.0, 312.0, 332.0, 352.0, 379.0, 392.0, 400.0,
     & 401.0, 405.0, 409.0/
C t7 thermocouple 7 (Assumed temperature at the top of the cup)
      data t7/ 300., 300., 300., 300., 300., 300., 300., 300.,
     & 300., 300., 300., 300., 300., 300., 300., 300., 300.,
     & 300., 300., 300./
```

A4top750

```
C z distance from bottom plate TC to CUP TC's
      data z/ 0.0, 0.48, 1.11, 2.38, 3.65, 4.92, 6.83,17.4/
C ts time in s
```

```
      data ts/ 0.0, 49.8, 74.8, 109.8, 119.8, 139.8, 174.8, 249.8,
     & 299.8, 374.8, 524.8, 604.8/
C t0 thermocouple 0 (bottom plate thermal couple)
      data t0/ 300.0, 309.6, 585.3, 964.6, 993.3, 1007.3, 1012.2,
     & 1012.7, 1014.0, 1013.6, 1013.8, 951.1/
C t1 thermocouple 1
      data t1/ 300.0, 300.0, 367.9, 618.4, 684.4, 774.8, 865.7,
     & 910.6, 921.0, 927.2, 902.7, 868.4/
C t2 thermocouple 2
      data t2/ 300.0, 300.0, 323.8, 477.3, 538.0, 645.2, 772.5,
     & 857.8, 875.8, 877.3, 850.6, 823.2/
C t3 thermocouple 3
      data t3/ 300.0, 300.2, 306.2, 362.0, 397.7, 483.8, 618.7,
     & 775.9, 810.9, 819.9, 794.1, 766.7/
C t4 thermocouple 4
      data t4/ 300.0, 300.3, 304.1, 329.0, 347.1, 416.9, 525.1,
     & 690.8, 752.1, 769.7, 754.3, 725.0/
C t5 thermocouple 5
      data t5/ 300.0, 300.7, 304.0, 319.8, 328.2, 376.8, 472.4,
     & 616.6, 663.1, 705.0, 710.3, 683.8/
C t6 thermocouple 6
      data t6/ 300.0, 301.6, 304.8, 313.5, 316.8, 330.2, 366.1,
     & 469.7, 504.1, 527.2, 590.4, 597.7/
C t7 thermocouple 7 (Assumed temperature at the top of the cup)
      data t7/ 300., 300., 300., 300., 300., 300., 300., 300., 300.,
     & 300., 300., 300./
```

A5bot750

```
C z distance from bottom plate TC to CUP TC's
      data z/ 0.0, 0.48, 1.11, 2.38, 3.65, 4.92, 6.83,17.4/
C ts time in s
      data ts/ 0.0, 148.5, 163.5, 173.5, 208.5, 223.5, 238.5, 253.5,
     & 283.5, 353.5, 433.5, 508.5, 603.5/
C t0 thermocouple 0 (bottom plate thermal couple)
      data t0/ 300.0, 304.6, 335.8, 398.1, 855.6, 943.0, 983.6,
     & 1001.4, 1013.0, 1014.3, 1015.9, 1015.9, 907.2/
C t1 thermocouple 1
      data t1/ 300.0, 305.3, 315.1, 334.2, 582.6, 683.3, 752.8,
     & 801.6, 846.4, 870.4, 879.6, 877.4, 809.4/
C t2 thermocouple 2
      data t2/ 300.0, 305.9, 308.5, 314.3, 436.3, 515.6, 585.2,
     & 645.8, 708.4, 752.2, 767.2, 766.3, 723.9/
C t3 thermocouple 3
      data t3/ 300.0, 306.7, 306.9, 307.6, 332.5, 364.2, 402.7,
     & 444.7, 510.6, 611.9, 655.5, 671.8, 642.2/
C t4 thermocouple 4
      data t4/ 300.0, 307.2, 307.4, 307.5, 312.7, 319.7, 332.0,
     & 350.7, 395.7, 474.1, 545.2, 585.0, 582.0/
C t5 thermocouple 5
      data t5/ 300.0, 307.2, 307.4, 307.6, 309.9, 311.8, 315.1,
     & 321.3, 343.9, 392.9, 444.8, 490.8, 515.3/
C t6 thermocouple 6
      data t6/ 300.0, 307.6, 307.7, 307.9, 309.5, 310.2, 310.8,
     & 311.9, 317.3, 336.3, 360.2, 389.2, 413.6/
C t7 thermocouple 7 (Assumed temperature at the top of the cup)
      data t7/ 300., 300., 300., 300., 300., 300., 300., 300., 300.,
```

```
     & 300., 300., 300., 300./
```

R6bot900-0

```
C z distance from bottom plate TC to CUP TC's
C bottom plate TC at 0.0, which is located 0.16 cm from foam surface
C Other Tc's located at 0.25, 0.5, 1.0, 1.5, 2.0, 2.5, 3.0, 4.0 inches
C            from foam/plate interface.  Thus, we need to convert these
C            numbers to cm and add 0.16 cm (14 cm is the top of the
can)
      data z/ 0.0,0.795,1.43,2.7,3.97,5.24,6.51,7.78,10.32,14.0/
C ts time in s
      data ts/ 0.0, 239.8, 249.8, 279.8, 309.8, 319.8, 339.8, 369.8,
     & 399.8, 409.8, 479.8, 539.8, 609.8/
C t0 thermocouple 0 (bottom plate thermal couple)
      data t0/ 319.4, 318.5, 391.7, 779.8, 1106.5, 1157.2, 1159.2,
     & 1153.9, 1153.3, 1153.4, 1151.9, 1015.6, 902.6/
C t1 thermocouple 1
      data t1/ 323.2, 322.7, 350.3, 565.4, 819.4, 884.5, 946.8,
     & 972.1, 980.5, 985.0, 990.3, 901.3, 809.1/
C t2 thermocouple 2
      data t2/ 324.5, 324.3, 330.2, 439.5, 627.0, 693.5, 772.0,
     & 813.9, 829.6, 835.9, 847.5, 792.6, 717.8/
C t3 thermocouple 3
      data t3/ 320.9, 320.6, 322.6, 345.6, 409.6, 440.3, 533.6,
     & 622.7, 653.9, 659.7, 684.9, 662.1, 606.4/
C t4 thermocouple 4
      data t4/ 315.6, 315.3, 317.0, 326.2, 347.0, 356.7, 389.0,
     & 468.3, 542.6, 555.2, 599.2, 593.4, 550.2/
C t5 thermocouple 5
      data t5/ 310.4, 310.3, 311.8, 318.5, 327.2, 330.8, 342.0,
     & 368.0, 420.0, 446.8, 518.9, 531.1, 508.5/
C t6 thermocouple 6
      data t6/ 306.3, 306.3, 307.7, 313.6, 319.2, 320.9, 325.9,
     & 334.4, 349.9, 358.8, 440.6, 475.7, 471.8/
C t7 thermocouple 7
      data t7/ 303.2, 303.1, 304.5, 309.7, 314.5, 315.8, 319.1,
     & 323.2, 329.0, 332.4, 367.3, 420.7, 435.4/
C t8 thermocouple 8
      data t8/ 298.3, 298.0, 299.3, 303.7, 307.3, 308.3, 310.1,
     & 312.0, 313.9, 314.7, 320.9, 328.2, 344.3/
C t9 thermocouple 9 (Assumed temperature at the top of the cup)
      data t9/ 300., 300., 300., 300., 300., 300., 300., 300.,
     & 300., 300., 300., 300., 300./
```

R8side750-0

```
C. . .DATA STATEMENTS. . . . . .
.
C z distance from bottom plate TC to CUP TC's
C bottom plate TC at 0.0, which is located 0.16 cm from foam surface
C Other Tc's located at 0.25, 0.5, 1.0, 1.5, 2.0, 2.5, 3.0, 4.0 inches
C            from foam/plate interface.  Thus, we need to convert these
C            numbers to cm and add 0.16 cm (14 cm is the top of the
can)
      data z/ 0.0,0.795,1.43,2.7,3.97,5.24,6.51,7.78,10.32,14.0/
C ts time in s
      data ts/ 0.0, 84.7, 94.7, 119.7, 144.7, 154.7, 164.7, 189.7,
```

```
     & 249.7, 299.7, 374.7, 434.7, 499.7/
C t0 thermocouple 0 (bottom plate thermal couple):  Array A, B, C, & D
      data t0/ 315.7, 317.1, 399.3, 691.2, 978.7, 1004.8, 1009.9,
     & 1002.7, 1002.2, 1005.0, 1005.2, 1004.6, 921.0/
C t1 thermocouple 1: Array A, B, C, & D
      data t1/ 326.3, 326.4, 355.4, 540.9, 778.2, 840.0, 867.9,
     & 896.4, 914.6, 908.4, 910.6, 913.4, 857.6/
C t2 thermocouple 2
      data t2/ 335.3, 334.3, 339.2, 420.8, 569.5, 647.9, 702.7,
     & 766.4, 812.0, 797.4, 807.1, 811.7, 782.7/
C t3 thermocouple 3
      data t3/ 339.6, 337.4, 338.4, 350.1, 395.1, 423.7, 459.9,
     & 573.1, 683.8, 688.3, 700.7, 704.3, 696.5/
C t4 thermocouple 4
      data t4/ 334.5, 332.5, 333.6, 334.4, 344.6, 352.3, 362.7,
     & 403.0, 558.8, 611.8, 636.5, 643.6, 645.8/
C t5 thermocouple 5
      data t5/ 328.0, 326.7, 327.9, 327.9, 330.8, 333.1, 335.4,
     & 347.3, 413.5, 513.6, 585.9, 605.8, 613.2/
C t6 thermocouple 6
      data t6/ 322.5, 321.8, 323.0, 322.9, 324.9, 325.8, 326.5,
     & 330.5, 350.3, 393.3, 517.4, 570.8, 587.6/
C t7 thermocouple 7
      data t7/ 317.7, 317.4, 318.7, 318.9, 320.9, 321.5, 321.5,
     & 323.3, 330.0, 344.4, 406.7, 511.6, 556.3/
C t8 thermocouple 8
      data t8/ 309.6, 309.3, 310.8, 311.3, 313.0, 313.2, 313.1,
     & 313.8, 315.5, 317.6, 325.6, 344.1, 389.6/
C t9 thermocouple 9 (Assumed temperature at the top of the cup)
      data t9/ 300., 300., 300., 300., 300., 300., 300., 300.,
     & 300., 300., 300., 300., 300./
```

R11top750-2

```
C z distance from bottom plate TC to CUP TC's
C bottom plate TC at 0.0, which is located 0.16 cm from foam surface
C Other Tc's located at 0.25, 0.5, 1.0, 1.5, 2.0, 2.5, 3.0, 4.0 inches
C           from foam/plate interface.  Thus, we need to convert these
C           numbers to cm and add 0.16 cm (14 cm is the top of the can)
      data z/ 0.0,0.795,1.43,2.7,3.97,5.24,6.51,7.78,10.32,14.0/
C ts time in s
      data ts/ 0.0, 129.8, 144.8, 189.8, 204.8, 244.8, 304.8, 399.9,
     & 454.8, 489.8, 529.8, 604.8/
C t0 thermocouple 0 (bottom plate thermal couple)
      data t0/ 316.8, 316.2, 437.7, 999.1, 1038.3, 1013.0, 1010.6,
     & 1011.0, 1011.1, 1010.3, 956.8, 859.8/
C t1 thermocouple 1
      data t1/ 318.5, 318.2, 364.1, 724.9, 811.4, 854.1, 870.3,
     & 877.4, 879.4, 871.7, 846.2, 764.9/
C t2 thermocouple 2
      data t2/ 317.8, 317.8, 333.8, 555.3, 648.2, 746.0, 785.6,
     & 801.7, 806.8, 797.9, 784.3, 714.2/
C t3 thermocouple 3
      data t3/ 313.0, 313.7, 321.3, 395.4, 435.3, 549.6, 658.9,
     & 704.2, 716.1, 711.1, 704.6, 650.7/
C t4 thermocouple 4
      data t4/ 307.4, 308.5, 316.0, 353.7, 367.4, 426.2, 513.6,
```

```
     & 617.7, 642.7, 644.7, 643.4, 603.4/
C t5 thermocouple 5
      data t5/ 303.1, 304.1, 311.6, 342.9, 348.6, 378.9, 423.3,
     & 499.7, 560.9, 580.7, 587.8, 563.3/
C t6 thermocouple 6
      data t6/ 299.7, 300.5, 308.3, 338.8, 342.0, 355.3, 377.6,
     & 407.4, 444.1, 471.5, 501.8, 514.1/
C t7 thermocouple 7
      data t7/ 297.0, 297.6, 305.4, 335.4, 337.7, 341.9, 352.4,
     & 363.6, 380.7, 391.9, 408.0, 437.3/
C t8 thermocouple 8
      data t8/ 293.9, 294.1, 301.0, 325.5, 326.2, 324.8, 326.4,
     & 328.1, 332.8, 333.9, 335.8, 340.7/
C t9 thermocouple 9 (Assumed temperature at the top of the cup)
      data t9/ 300., 300., 300., 300., 300., 300., 300., 300.,
     & 300., 300., 300., 300./
```

R14bot750-2

```
C z distance from bottom plate TC to CUP TC's
C bottom plate TC at 0.0, which is located 0.16 cm from foam surface
C Other Tc's located at 0.25, 0.5, 1.0, 1.5, 2.0, 2.5, 3.0, 4.0 inches
C          from foam/plate interface.  Thus, we need to convert these
C          numbers to cm and add 0.16 cm (14 cm is the top of the can)
      data z/ 0.0,0.795,1.43,2.7,3.97,5.24,6.51,7.78,10.32,14.0/
C ts time in s
      data ts/ 0.0, 44.8, 54.8, 104.8, 154.8, 199.8, 259.8, 359.8,
     & 389.8, 499.8, 604.8/
C t0 thermocouple 0 (bottom plate thermal couple)
      data t0/ 296.0, 298.7, 438.5, 1058.9, 1025.1, 1022.9, 1023.3,
     & 1021.6, 1018.5, 858.5, 756.0/
C t1 thermocouple 1
      data t1/ 300.0, 299.3, 326.0, 738.8, 818.4, 837.8, 848.2,
     & 854.7, 842.0, 738.2, 657.6/
C t2 thermocouple 2
      data t2/ 298.3, 299.3, 305.7, 555.3, 688.2, 712.3, 735.9,
     & 751.7, 736.8, 663.9, 594.8/
C t3 thermocouple 3
      data t3/ 298.3, 299.2, 300.2, 355.8, 464.7, 508.9, 576.1,
     & 624.5, 601.5, 567.6, 511.1/
C t4 thermocouple 4
      data t4/ 298.8, 299.7, 300.6, 314.7, 364.8, 395.4, 443.6,
     & 535.8, 556.8, 527.7, 480.1/
C t5 thermocouple 5
      data t5/ 298.6, 299.8, 300.8, 308.0, 327.3, 345.4, 368.3,
     & 436.1, 472.4, 469.9, 441.6/
C t6 thermocouple 6
      data t6/ 297.9, 299.0, 300.1, 306.2, 312.8, 321.5, 332.2,
     & 362.5, 376.2, 407.9, 401.6/
C t7 thermocouple 7
      data t7/ 297.0, 297.8, 298.9, 304.4, 307.4, 311.7, 317.9,
     & 332.0, 337.2, 356.8, 362.7/
C t8 thermocouple 8
      data t8/ 296.1, 296.6, 297.6, 301.9, 302.9, 303.9, 305.9,
     & 310.4, 311.2, 312.7, 315.6/
C t9 thermocouple 9 (Assumed temperature at the top of the cup)
      data t9/ 300., 300., 300., 300., 300., 300., 300., 300.,
```

```
     & 300., 300., 300./
```

R20top750-4

```
C z distance from bottom plate TC to CUP TC's
C bottom plate TC at 0.0, which is located 0.16 cm from foam surface
C Other Tc's located at 0.25, 0.5, 1.0, 1.5, 2.0, 2.5, 3.0, 4.0 inches
C           from foam/plate interface.  Thus, we need to convert these
C           numbers to cm and add 0.16 cm (14 cm is the top of the can)
      data z/ 0.0,0.795,1.43,2.7,3.97,5.24,6.51,7.78,10.32,14.0/
C ts time in s
      data ts/ 0.0, 199.8, 219.8, 259.8, 269.8, 279.8, 319.8, 399.8,
     & 449.8, 549.9, 729.8, 799.8/
C t0 thermocouple 0 (bottom plate thermal couple)
      data t0/ 300.0, 310.9, 499.7, 1027.3, 1062.4, 1058.1, 1021.6,
     & 1018.8, 1019.0, 1019.9, 1018.3, 925.6/
C t1 thermocouple 1
      data t1/ 300.0, 317.0, 397.9, 746.2, 810.1, 843.9, 878.6, 896.9,
     & 895.0, 904.1, 904.5, 838.4/
C t2 thermocouple 2
      data t2/ 300.0, 319.0, 349.5, 577.7, 646.8, 696.1, 771.8, 809.1,
     & 810.3, 826.1, 828.6, 774.4/
C t3 thermocouple 3
      data t3/ 300.0, 319.1, 322.6, 379.9, 408.9, 440.9, 564.6, 674.7,
     & 694.3, 721.6, 732.1, 690.6/
C t4 thermocouple 4
      data t4/ 300.0, 316.1, 318.0, 328.2, 335.0, 344.2, 397.2, 526.0,
     & 589.7, 642.6, 664.9, 632.4/
C t5 thermocouple 5
      data t5/ 300.0, 312.8, 314.5, 317.7, 319.5, 321.9, 341.5, 407.1,
     & 460.6, 566.8, 615.4, 590.0/
C t6 thermocouple 6
      data t6/ 300.0, 309.7, 311.2, 313.3, 313.9, 314.5, 320.9, 349.2,
     & 375.1, 450.6, 561.2, 548.1/
C t7 thermocouple 7
      data t7/ 300.0, 306.8, 308.1, 310.1, 310.5, 310.7, 313.1, 324.5,
     & 336.4, 373.2, 467.9, 482.1/
C t8 thermocouple 8
      data t8/ 300.0, 302.3, 303.7, 305.5, 305.7, 305.8, 306.7, 309.5,
     & 312.7, 323.2, 351.1, 358.1/
C t9 thermocouple 9 (Assumed temperature at the top of the cup)
      data t9/ 300., 300., 300., 300., 300., 300., 300., 300.,
     & 300., 300., 300.,300./
```

R22bot600-4

```
C z distance from bottom plate TC to CUP TC's
C bottom plate TC at 0.0, which is located 0.16 cm from foam surface
C Other Tc's located at 0.25, 0.5, 1.0, 1.5, 2.0, 2.5, 3.0, 4.0 inches
C           from foam/plate interface.  Thus, we need to convert these
C           numbers to cm and add 0.16 cm (14 cm is the top of the can)
      data z/ 0.0,0.795,1.43,2.7,3.97,5.24,6.51,7.78,10.32,14.0/
C ts time in s
      data ts/ 0.0, 94.7, 154.7, 174.7, 219.7, 299.7, 374.7,
     & 449.7, 644.7/
C t0 thermocouple 0 (bottom plate thermal couple)
      data t0/ 300.0, 306.0, 842.7, 874.4, 862.6, 863.8, 865.2,
     & 863.9, 864.1/
```

```
C t1 thermocouple 1
      data t1/ 300.0, 308.7, 635.3, 713.7, 749.2, 763.2, 770.8,
     & 767.6, 777.8/
C t2 thermocouple 2
      data t2/ 300.0, 312.3, 492.0, 575.6, 636.4, 661.5, 681.7,
     & 673.1, 700.2/
C t3 thermocouple 3
      data t3/ 300.0, 315.0, 365.7, 407.5, 482.3, 557.2, 585.0,
     & 595.8, 625.8/
C t4 thermocouple 4
      data t4/ 300.0, 316.8, 332.9, 344.3, 388.1, 443.7, 514.3,
     & 552.1, 577.1/
C t5 thermocouple 5
      data t5/ 300.0, 317.1, 327.6, 330.0, 350.7, 377.3, 429.0,
     & 499.4, 537.5/
C t6 thermocouple 6
      data t6/ 300.0, 317.2, 326.9, 327.1, 335.6, 348.7, 380.0,
     & 419.2, 497.7/
C t7 thermocouple 7
      data t7/ 300.0, 317.5, 327.1, 326.6, 329.5, 336.2, 357.1,
     & 377.5, 438.9/
C t8 thermocouple 8
      data t8/ 300.0, 315.7, 324.2, 323.1, 322.6, 324.5, 335.9,
     & 343.6, 359.1/
C t9 thermocouple 9 (Assumed temperature at the top of the cup)
      data t9/ 300., 300., 300., 300., 300., 300., 300., 300., 300./
```

R23bot750-4

```
C z distance from bottom plate TC to CUP TC's
C bottom plate TC at 0.0, which is located 0.16 cm from foam surface
C Other Tc's located at 0.25, 0.5, 1.0, 1.5, 2.0, 2.5, 3.0, 4.0 inches
C          from foam/plate interface.  Thus, we need to convert these
C          numbers to cm and add 0.16 cm (14 cm is the top of the can)
      data z/ 0.0,0.795,1.43,2.7,3.97,5.24,6.51,7.78,10.32,14.0/
C ts time in s
      data ts/ 0.0, 39.8, 49.8, 94.8, 109.8, 129.8, 164.8, 199.8,
     & 249.8, 299.8, 329.8, 364.8/
C t0 thermocouple 0 (bottom plate thermal couple)
      data t0/ 300.0, 308.0, 422.0, 977.9, 1031.4, 1020.8, 1008.7,
     & 1009.4, 1011.1, 1011.4, 1010.4, 963.5/
C t1 thermocouple 1
      data t1/ 300.0, 303.1, 337.1, 677.5, 770.9, 814.9, 842.8,
     & 857.9, 863.1, 874.7, 875.9, 854.7/
C t2 thermocouple 2
      data t2/ 300.0, 300.5, 307.7, 516.3, 606.6, 669.5, 718.2,
     & 736.0, 731.4, 753.0, 750.3, 737.0/
C t3 thermocouple 3
      data t3/ 300.0, 297.7, 298.4, 353.0, 393.2, 452.0, 533.7,
     & 581.5, 594.8, 621.0, 618.6, 613.0/
C t4 thermocouple 4
      data t4/ 300.0, 296.1, 296.5, 312.8, 324.9, 350.8, 404.9,
     & 454.9, 512.2, 568.8, 572.4, 566.6/
C t5 thermocouple 5
      data t5/ 300.0, 295.0, 295.4, 302.9, 306.2, 314.5, 341.5,
     & 374.1, 401.8, 479.9, 521.8, 535.7/
C t6 thermocouple 6
```

```
      data t6/ 300.0, 294.2, 294.5, 300.2, 301.4, 304.1, 317.1,
     & 336.0, 348.4, 389.3, 416.2, 452.5/
C t7 thermocouple 7
      data t7/ 300.0, 293.7, 294.0, 299.1, 299.8, 300.9, 308.5,
     & 319.8, 324.1, 345.5, 355.7, 371.9/
C t8 thermocouple 8
      data t8/ 300.0, 292.8, 293.2, 297.2, 297.6, 298.0, 302.1,
     & 307.5, 306.0, 314.5, 315.7, 318.7/
C t9 thermocouple 9 (Assumed temperature at the top of the cup)
      data t9/ 300., 300., 300., 300., 300., 300., 300., 300.,
     & 300., 300., 300., 300./
```

T2top925-d20

```
C z distance from bottom plate TC to CUP TC's
C bottom plate TC at 0.0, which is located 0.16 cm from foam surface
C Other Tc's located at 0., .875, 2.78, 4.05, 4.45 cm
      data z/ 0.0,0.875,2.78, 4.05, 4.45/
C ts time is s
      data ts/ 0.0, 59.9, 99.9, 199.9, 233.9, 251.9, 289.9, 299.9,
     & 335.9, 439.9/
C t0 thermocouple 0 (bottom plate thermocouple)
      data t0/ 300.0, 286.7, 456.4, 842.5, 974.0, 1044.5, 1189.0,
     & 1205.1, 1197.3, 1194.3/
C t1 thermocouple 1
      data t1/ 300.0, 286.5, 308.7, 490.6, 606.9, 701.8, 782.8,
     & 802.0, 840.0, 863.7/
C t2 thermocouple 2
      data t2/ 300.0, 286.7, 290.6, 358.0, 460.1, 513.8, 573.0,
     & 584.6, 615.0, 660.6/
C t3 thermocouple 3
      data t3/ 300.0, 286.7, 288.3, 310.7, 367.7, 402.3, 431.2,
     & 435.7, 451.4, 498.4/
C t4 thermocouple 4 (top of can)
      data t4/ 300.0, 286.3, 287.0, 290.6, 293.4, 295.8, 305.6,
     & 309.0, 319.6, 340.9/
```

T3top925-d8

```
C z distance from bottom plate TC to CUP TC's
C bottom plate TC at 0.0, which is located 0.16 cm from foam surface
C Other Tc's located at 0., .875, 2.78, 4.05, 4.45 cm
      data z/ 0.0,0.875,2.78, 4.05, 4.45/
C ts time is s
      data ts/ 0.0, 73.9, 149.9, 199.9, 249.9, 303.9, 315.9, 343.9,
     & 399.9, 485.9/
C t0 thermocouple 0 (bottom plate thermocouple)
      data t0/ 300.0, 288.9, 589.2, 781.3, 978.1, 1180.6, 1205.4,
     & 1198.2, 1193.3, 1192.9/
C t1 thermocouple 1
      data t1/ 300.0, 289.3, 359.8, 457.8, 588.2, 746.7, 794.5,
     & 850.7, 875.0, 864.7/
C t2 thermocouple 2
      data t2/ 300.0, 289.4, 306.2, 344.0, 403.1, 502.9, 567.6,
     & 623.0, 653.3, 645.2/
C t3 thermocouple 3
      data t3/ 300.0, 289.4, 294.9, 308.6, 334.7, 396.1, 443.1,
     & 475.2, 489.6, 495.4/
```

```
C t4 thermocouple 4 (top of can)
      data t4/ 300.0, 288.9, 290.4, 292.4, 295.7, 303.1, 306.0,
   & 316.2, 343.0, 380.3/
```

T4top925-08

```
C z distance from bottom plate TC to CUP TC's
C bottom plate TC at 0.0, which is located 0.16 cm from foam surface
C Other Tc's located at 0., .875, 2.78, 4.05, 4.45 cm
      data z/ 0.0,0.875,2.78, 4.05, 4.45/
C ts time is s
      data ts/ 0.0, 53.9, 75.9, 125.9, 225.9, 269.9,
     & 285.9, 335.9, 361.9/
C t0 thermocouple 0 (bottom plate thermocouple)
      data t0/ 281.9, 285.5, 386.4, 585.1, 967.9,
     & 1138.3, 1200.2, 1194.8, 1190.9/
C t1 thermocouple 1
      data t1/ 282.1, 282.0, 290.8, 369.4, 616.2,
     & 718.6, 773.8, 871.7, 891.2/
C t2 thermocouple 2
      data t2/ 281.9, 281.9, 283.7, 308.3, 442.4,
     & 489.4, 520.5, 637.1, 663.1/
C t3 thermocouple 3
      data t3/ 281.8, 281.7, 282.8, 289.3, 351.5,
     & 368.8, 381.3, 439.8, 463.6/
C t4 thermocouple 4 (top of can)
      data t4/ 281.2, 281.2, 281.8, 283.4, 290.9,
     & 441.3, 451.0, 456.8, 480.6/
```

T5top925-020

```
C z distance from bottom plate TC to CUP TC's
C bottom plate TC at 0.0, which is located 0.16 cm from foam surface
C Other Tc's located at 0., .875, 2.78, 4.05, 4.45 cm
      data z/ 0.0,0.875,2.78, 4.05, 4.45/
C ts time is s
      data ts/ 0.0, 71.9, 149.9, 275.9, 299.9, 319.9, 385.9, 499.9,
     & 699.9, 1203.9/
C t0 thermocouple 0 (bottom plate thermocouple)
      data t0/ 300.0, 287.9, 593.7, 1082.1, 1172.2, 1201.2, 1189.9,
     & 1193.9, 1190.9, 1191.6/
C t1 thermocouple 1
      data t1/ 300.0, 288.0, 368.1, 640.8, 688.0, 728.4, 787.5, 846.2,
     & 877.9, 907.8/
C t2 thermocouple 2
      data t2/ 300.0, 287.9, 311.9, 453.2, 480.7, 502.1, 548.6, 606.2,
     & 664.8, 732.2/
C t3 thermocouple 3
      data t3/ 300.0, 287.6, 295.0, 358.9, 373.1, 384.3, 412.4, 455.3,
     & 503.7, 586.3/
C t4 thermocouple 4 (top of can)
      data t4/ 300.0, 287.2, 290.1, 338.3, 392.2, 409.2, 462.9, 485.3,
     & 492.2, 518.2/
```

V750mean

```
C z distance from bottom plate TC to CUP TC's
C bottom plate TC at 0.0, which is located 0.71 cm from foam surface
```

```
C 0.75*(.375") = .28125" or 0.714375 cm
C Other Tc's located at 0., 1.98, 3.25, 4.52, 5.79, 7.77 cm
      data z/ 0.0, 1.98, 3.25, 4.52, 5.79, 7.77/
C ts time is s
      data ts/ 0.0, 36.0, 60.0, 120.0, 180.0, 282.0, 296.0, 336.0,
     & 374.0, 468.0, 666.0, 750.0, 1500.0, 2186.0, 2284.0/
C t0 thermocouple 0 (h_plate thermocouple)
      data t0/ 288.8, 289.9, 373.5, 554.9, 731.3, 1027.9, 1034.5,
     & 1024.1, 1020.9, 1021.6, 1021.8, 1021.5, 1021.7, 1020.5, 887.1/
C t1 thermocouple 1
      data t1/ 287.5, 287.5, 291.7, 330.6, 394.2, 548.3, 571.2, 619.6,
     & 644.2, 674.8, 692.6, 695.2, 692.3, 696.3, 649.6/
C t2 thermocouple 2
      data t2/ 287.4, 287.4, 290.7, 307.8, 340.0, 422.8, 434.3, 466.4,
     & 490.9, 535.7, 577.5, 585.6, 597.9, 606.7, 577.5/
C t3 thermocouple 3
      data t3/ 287.4, 287.4, 290.7, 300.8, 317.1, 361.8, 367.6, 384.1,
     & 399.8, 430.3, 467.8, 478.0, 508.6, 524.0, 510.8/
C t4 thermocouple 4
      data t4/ 287.6, 287.7, 290.9, 297.8, 306.6, 330.5, 332.9, 339.7,
     & 347.9, 366.3, 391.8, 400.3, 439.2, 462.4, 458.0/
C t5 thermocouple 5 (c_plate thermocouple)
      data t5/ 288.5, 288.4, 288.8, 290.3, 292.3, 297.1, 297.8, 299.4,
   & 300.8, 304.8, 316.7, 322.9, 384.4, 425.8, 429.6/
```

V900mean

```
C z distance from bottom plate TC to CUP TC's
C bottom plate TC at 0.0, which is located 0.71 cm from foam surface
C 0.75*(.375") = .28125" or 0.714375 cm
C Other Tc's located at 0., 1.98, 3.25, 4.52, 5.79, 7.77 cm
      data z/ 0.0, 1.98, 3.25, 4.52, 5.79, 7.77/
C ts time is s
      data ts/ 0.0, 36.0, 38.0, 96.0, 180.0, 300.0, 330.0, 338.0,
     & 400.0, 510.0, 660.0, 900.0, 1500.0, 2122.0, 2208.0, 2332.0/
C t0 thermocouple 0 (h_plate thermocouple)
      data t0/ 294.9, 295.7, 300.4, 490.5, 746.3, 1105.4, 1187.0,
     & 1188.2, 1174.4, 1173.0, 1173.0, 1172.9, 1173.1, 1173.2,
     & 1002.6, 850.9/
C t1 thermocouple 1
      data t1/ 294.1, 294.2, 294.3, 316.7, 402.8, 590.8, 653.9,
     & 671.0, 742.0, 778.7, 788.2, 793.6, 795.5, 799.4, 735.4, 643.5/
C t2 thermocouple 2
      data t2/ 294.0, 293.9, 294.1, 305.0, 346.9, 448.3, 483.5,
     & 493.4, 562.3, 631.9, 658.0, 671.3, 679.8, 690.3, 649.4, 580.4/
C t3 thermocouple 3
      data t3/ 293.9, 293.9, 294.1, 302.2, 323.5, 379.8, 399.5,
     & 404.7, 443.1, 499.5, 532.5, 558.2, 584.3, 604.5, 581.5, 534.1/
C t4 thermocouple 4
      data t4/ 294.0, 294.0, 294.2, 300.7, 311.9, 341.9, 352.9,
     & 355.2, 373.6, 407.8, 432.4, 457.9, 499.7, 530.8, 522.3, 498.9/
C t5 thermocouple 5 (c_plate thermocouple)
      data t5/ 294.4, 294.3, 294.4, 295.5, 298.0, 303.9, 306.0,
     & 306.6, 310.2, 318.1, 332.2, 359.4, 430.3, 486.6, 490.7, 492.9/
```

Appendix

Intentionally left blank

References

1. Hobbs M.L., "SREF—A simple removable epoxy foam decomposition chemistry model," Sandia National Laboratories Report 2003-4550, Albuquerque, NM (Dec 2003).

2. Bova S.W., Glass M.W., Dowding K.J., Lober R.R., Cochran R.J., "CALORE, A Computational Heat Transfer Program: Volume I Theory Manual," Sandia National Laboratories Report SANDTBD, Albuquerque, NM (In Review).

3. Erickson, K.E., Trujillo, S.M., Thompson, K.R., Sun, A.C., Hobbs, M.L., and Dowding, K.J., "Liquefaction and flow behavior of a thermally decomposing removable epoxy foam," in *Computational Methods in Materials Characterisation*, Edited by Mammoli, A.A. and Brebbia, C.A., WIT Press, Southampton, UK, 217 (2004).

4. Erickson, K.L., Trujillo, S.M., Oelfke, J.B., Hanks, C.R., Belone, and Ramirez, D.M., "Component-Scale Removable Epoxy Foam (REF) Thermal Decomposition Experiments ("MFER" series, April 2003) Supporting the FY04/Q2 Level 1 V&V Milestone. Part1: Temperature Data," Sandia National Laboratories Report SANDTBD (In preparation, 2004).

5. Hobbs M.L., Erickson K.L., Chu T.Y., "Modeling decomposition of unconfined rigid polyurethane foam," *Polym Degrad Stab,* **69**, 47, (2000).

6. Hobbs M.L., Erickson K.L., Chu T.Y., Borek T.T., Thompson K.R., Dowding K.J., Clayton D., Fletcher T.H., "CPUF—A Chemical-structure-based PolyUrethane Foam decomposition and foam response model," Sandia National Laboratories report SAND2003-2282, Albuquerque, NM (2003).

7. Hobbs M.L. and Lemmon G.H., "SPUF—A Simple PolyUrethane Foam Mass Loss and Response Model," Sandia National Laboratories report SAND2003-2099, Albuquerque, NM (2003). See also Hobbs, M.L. and Lemmon, G.H., "Polyurethane foam response to fire in practical geometries," accepted for publication in *Polymer Degradation and Stability* (Oct. 2003).

8. McElhanon J.R., Russick E.M., Wheeler D.R., Loy D.A., and Aubert J.H., "Removable Foams Based on an Epoxy Resin Incorporating Reversible Diels-Alder Adduct," *J. Appl.Polym. Sci.*, **85**, 1496 (2002).

9. Dobranich D. and Gill W., "A Thermal Model Validation Test Unit for the W76-1 AF&F—Design, Experiments, and Simulations," Sandia National Laboratories report SAND2002-1769, Albuquerque, NM (2002).

10. Aselage, T.L., "C_p Measurements for Removable Epoxy Foam," EMAIL to Hobbs, M.L., (September 18, 2001).

11. Gembarovic J. and Taylor R.E., "Thermophysical Properties of Plastic Sample—A Report to Sandia National Laboratories," Thermophysical Properties Research Laboratory, Inc. report TPRL2868, West Lafayette, IN (October 2003).

12. Incropera F.P. and DeWitt D.P., *Fundamentals of Heat and Mass Transfer*, Fifth Edition, John Wiley & Sons, New York (2002).

13. Reid R.C., Prausnitz J.M., and Poling, B.E., *The Properties of Gases & Liquids*, Fourth Edition, McGraw-Hill Book Company, New York (1987).

14. Sethian J.A., *Level Set Methods and Fast Marching Methods*. Cambridge University Press, Cambridge (1999).

15. Sun, A.C., Erickson, K.L, Hobbs, M.L., Adolf, D., and Stavig, M., "Modeling multiphase flow of liquefied removable epoxy foam," in *Computational Methods in Materials Characterisation*, Edited by Mammoli, A.A. and Brebbia, C.A., WIT Press, Southampton, UK, 197 (2004).

16. Collishaw, P.G., and Evans, J.R.G., "Review—An Assessment of Expressions for the Apparent Thermal Conductivity of Cellular Materials," *Journal of Material Science*, **29**, 2261-22723 (1994).

Distribution

Brigham Young University (1)
Department of Chemical Engineering
Attn: Dr. Thomas H. Fletcher
350 K Clyde Building
Provo, Utah 84602-4100

Easterling Statistical Consulting (1)
51 Avenida del Sol
Cedar Crest, NM 87008

Federal Aviation Administration (1)
Attn: Richard E. Lyon
Fire Safety Section, AAR-422
William J. Hughes Technical Center
Atlantic City International Airport, NJ 08405

New Mexico State University (1)
Department of Mechanical Engineering
Attn: Richard G. Hills
Las Cruces, New Mexico 88003

United States Department of Commerce (1)
Attn: Kathryn M. Butler
Building and Fire Research Laboratory
National Institute of Standards and Technology
Gaithersburg, MD 20899

University of California, Berkeley (1)
Attn: Carlos Fernandez-Pello
Mechanical Engineering Department
6105a Etcheverry Hall
University of California
Berkeley, CA 94720

University of Utah (1)
Attn: Ronald Pugmire
Associate Vice President for Research
Professor of Chemical & Fuels Engineering
210 Park Building
Salt Lake City, UT 84112

University of Utah (1)
Attn: David M. Grant
Distinguished Professor of Chemistry
Henry Eyring Bldg
315 S 1400 East Rm 2020
Salt Lake City, UT 84112

University of Washington (1)
Dept of Mechanical Engineering
Attn: Ashley Emery
Box 352600
Seattle, WA 98195-2600

Sandia

1	MS0888	1811	R. L. Clough
1	MS0888	1811	J. H. Aubert
1	MS0888	1811	E. M. Russick
1	MS0886	1822	R. P. Goehner
1	MS0886	1822	T. T. Borek
1	MS0888	1832	N. R. Sorenson
1	MS1411	1834	A. L. Frischknecht
1	MS0481	2132	R. J. Harrison
1	MS0481	2132	D. R. Helmich
1	MS0427	2134	R. A. Paulsen, Jr.
1	MS0481	2137	T. F. Hendrickson
1	MS0521	2520	M. R. Prairie
1	MS0613	2525	T. L. Aselage
1	MS1454	2554	A. M. Renlund
1	MS1455	2555	L. G. Minier
1	MS0374	2991	J. W. Shelton, III
1	MS9014	8242	D. M. Kwon
1	MS9014	8242	A. R. Ortega
1	MS9042	8752	C. D. Moen
1	MS9042	8752	R. H. Nilson
1	MS0384	9100	C. W. Peterson
1	MS0836	9100	M. R. Baer
1	MS1393	9100	T. Y. Chu (in Washington DC, Forrestal Building)
1	MS0826	9100	D. K. Gartling
1	MS0825	9110	W. L. Hermina
1	MS0834	9112	J. E. Johannes
1	MS0834	9112	K. L. Erickson
1	MS0834	9112	S. M. Trujillo
1	MS1310	9113	S. N. Kempka
1	MS0834	9114	T. A. Baer
1	MS0834	9114	P. L. Hopkins
1	MS0834	9114	A. M. Kraynik
1	MS0834	9114	P. R. Schunk
1	MS0834	9114	A. C. Sun
1	MS0836	9116	E. S. Hertel
1	MS0836	9116	B. L. Bainbridge
1	MS0836	9116	B. D. Boughton
1	MS0836	9116	J. F. Dempsey
1	MS0836	9116	D. D. Dobranich
1	MS0836	9116	R. C. Dykhuizen
1	MS0836	9116	N. D. Francis, Jr.
5	MS0836	9116	M. L. Hobbs
1	MS0836	9116	R. E. Hogan
1	MS0836	9116	R. G. Schmitt
1	MS0836	9117	R. O. Griffith
1	MS0836	9117	M. E. Larsen
1	MS0555	9122	M. S. Garrett
1	MS0555	9122	K. R. Thompson

1	MS0893	9123	M. K. Neilsen
1	MS0824	9130	J. L. Moya
1	MS0821	9132	L. A. Gritzo
1	MS0836	9132	W. Gill
1	MS1135	9132	J. T. Nakos
1	MS0836	9132	C. Romero
1	MS1135	9132	J. M. Suo-Anttila
1	MS1135	9132	S. R. Tieszen
1	MS0828	9133	M. Pilch
1	MS0828	9133	K. J. Dowding
1	MS0828	9133	V. J. Romero
1	MS0828	9133	W.L. Oberkampf
1	MS0384	9140	H. S. Morgan
1	MS0382	9141	E. A. Boucheron
1	MS0382	9141	S. W. Bova
1	MS0382	9141	M. W. Glass
1	MS0382	9141	R. R. Lober
1	MS0370	9211	M. S. Eldred
1	MS0370	9211	T. G. Trucano
1	MS0151	9750	A. C. Ratzel
1	MS0139	9900	M. O. Vahle
1	MS0139	9905	S. E. Lott
1	MS0829	12323	B. M. Rutherford
1	MS0405	12333	T. R. Jones
1	MS0405	12333	L. A. Schoof
1	MS0405	12333	S. E. Camp

1	MS9018	8945-1	Central Technical Files
2	MS0899	9619	Technical Library